MODELLING AND SIMULATING VOLTAGE CONTROLLED MAGNETIC ANISOTROPY MAGNETIC MEMORY DEVICES

by

Wilson Zhu

Senior Thesis in Electrical Engineering
University of Illinois at Urbana-Champaign
Advisor: Shaloo Rakheja
May 2022

ABSTRACT

Magnetoresistive random access memory (MRAM) devices offer non-volatile memory storage due to them storing bits with magnetic spin instead of with electrical charge, meaning they can offer long term digital memory storage without leaking energy while idle. This is potentially a huge advantage as digital technology continues to include increasing numbers of transistors. Furthermore, MRAM is a very promising solution that can replace long memory storage devices such as NAND flash memories, and can potentially become a universal memory that replaces DRAM and even SRAM due to its comparable dynamic power consumption and its ability to be interfaced with silicon fabrication methods and materials. Both theoretical and experimental research in the area of magnets has already proven the viability of MRAM in Spin transfer torque (STT) MRAM devices, which already have on the market options for commercial use. Another type of MRAM known as voltage controlled magnetic anisotropy (VCMA) can be used as an extension to STT devices that can lower dynamic energy consumption even further while providing faster switching times. In this thesis I first summarize the basic magnetic theory necessary to understand VCMA devices. I then describe the basics of STT devices and the currently most accepted theory behind VCMA devices, where research is still ongoing. I conclude with simulations of a singular VCMA memory device during its write process of switching a zero bit to a one bit and vice versa through Python.

Subject Keywords: Circuits and Systems; Circuit Simulation; Magnetic Circuits; Magnetic Memory; Spintronics

To math team.

ACKNOWLEDGMENTS

I reached out to Professor Rakheja at the beginning of fall semester in search of an advisor for a senior thesis project. I am very grateful to have found a topic that although was very challenging to research, is also a topic that continues to pique my interest while also being relevant and practical. Thank you for your encouragement to always try my best.

I would also like to extend a special thanks to the members in Professor Rakheja's research group: Ankit Shukla, Siyuan Qian, and Laura Heller for answering all of my questions on magnetic devices; and Yicong Dong and Ashwin Tunga.

TABLE OF CONTENTS

LIST OF FIGURES

CHAPTER 1

INTRODUCTION

1.1 Why Magnetic Random Access Memory?

One of the major challenges facing computing today is memory bottleneck: computing intensive problems where the processor needs to access memory on a separate chip often take up the most time and have large power consumption [1]. In particular, semiconductor memories experience a major problem due to static energy consumption caused by leakage currents [2], [3]. A lot of research is being done to reduce memory bottleneck, including neuromorphic computing and alternative memory storage devices such as ferroelectric memory, phase change memory, and magnetic memory, all of which have on-the-market options, but are still in development [4]. In this paper, we explore voltage controlled magnetic anisotropy (VCMA) magnetoresistive random access memory (MRAM) devices and compare them to their spin transfer torque (STT) counterparts in terms of switching times. MRAMs in general are non-volatile storage devices that have less passive energy leakage than traditional memories, meaning they can store digital information for long periods of time without needing a power source to maintain bit retention. This is because MRAM uses spintronics to store logic "zero" and logic "one" states with magnetic spin instead of electric charge. MRAMs can also be more area efficient that on-chip SRAM while still offering competitive speeds, and can easily integrate into silicon manufacturing technologies and materials, therefore providing their potential to be universal memory devices [5].

1.2 Types of Magnetic Random Access Memory

MRAM devices consist of a reference layer where the magnetization is fixed in a certain direction, and a free layer where the magnetization direction is manipulated and changed. There are currently three different types of MRAM devices being researched, with their differences lying in how memory writes can be performed to change the magnetization direction of the free layer: Spin transfer torque (STT), spin orbit torque (SOT) and voltage controlled magnetic anisotropy (VCMA) memory devices. The following section will briefly explain some of the features, benefits, and drawbacks of these three devices and effects. A simple representation of these three devices can be seen in Figure 1.1.

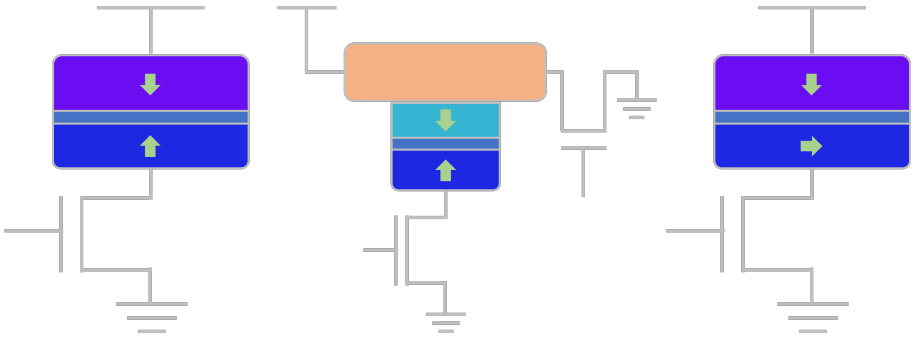

Figure 1.1: A simplified representation of three different types of MRAM devices. The green arrows represent the magnetic anisotropy, or preferred magnetization direction of the metal magnet layers at a specific moment in time. From left: STT, SOT, VCMA.

The origin of the ability for MRAMs to act as memory devices lies in the tunneling magnetoresistance (TMR) effect, which is related to the giant magnetoresistance effect (GMR) used in hard disk drives (HDDs): two magnetic layers with different magnetization directions exhibit an electrical resistance dependent on the angle between them [6], [7], [8], [9]. Magnetizations in a parallel orientation have a minimum resistance, while magnetizations with an antiparallel orientation have a maximum resistance. The resistance relationship is approximately expressed in Equation 1.1:

$$R(\theta) = \frac{R_{AP} + R_P}{2} - \frac{R_{AP} - R_P}{2} \times \cos(\theta) \tag{1.1}$$

where R_{AP} is the maximum resistance when the magnetizations are antipar-

allel, R_P is the minimum resistance when the magnetizations are parallel, and θ is the angle between the two magnetizations of the two magnets.

By passing a small read current that does not disturb the magnetization direction of the free layer through any of the three MRAM types, a voltage difference can be measured across the memory devices and read out as a "one" or "zero."

1.2.1 Spin Transfer Torque

STT devices are the simplest MRAM devices and are the furthest along in terms of development with on-the-market options [10]. For STT devices, A charge current or a voltage that causes a charge current is sent through the magnet [6], [11]. As this charge current passes through the reference layer of the magnet structure, it becomes polarized into a spin current that aligns itself parallelly(antiparallelly) to the the magnetization direction of the reference layer with a negative(positive) current. This spin polarized current then imparts a torque on the magnetization direction of the free layer, aligning the magnetization direction of the free layer in the same direction as the spin current, performing the desired write operation.

Some features or drawbacks of STT devices are as follows. STT devices require bidirectional currents or voltage levels to switch between bit states, meaning a different sign of current is required to switch from "zero" to "one" compared to from "one" to "zero." Furthermore, The read and write paths travel through the magnet in the same path, which means that a third weaker voltage level is required to read versus write. Finally, STT has higher dynamic energy consumption compared to other switching methods.

1.2.2 Spin Orbit Torque

SOT devices are similar to STT devices except that the spin currents are generated within one magnet instead of being passed from another magnet. Special heavy metal materials such as transition metal dichalcogenide topological insulators produce spin torques through the spin hall effect, orbital

hall effect, or the Rashba-Edelstein effect [1], [12]. This means that the write current passes through a different path than the read current and that SOT devices are 3-terminal devices as shown in Figure 1.1. The main advantage of SOT devices over STT devices is that the conversion efficiency factor of charge current to spin current, also known as the spin polarization coefficient, can be > 1, meaning that SOT devices can have lower dynamic energy consumption than STT devices.

1.2.3 Voltage Controlled Magnetic Anisotropy

VCMA devices add an additional element of control over magnetic anisotropy, or preferred magnetization direction, through magnetoelectric effects: an applied voltage or electric field can directly affect the magnetization rather than relying on a spin current to torque the magnet's magnetization direction. There are a couple of types possible, but for this thesis I will be focusing on VCMA effects with the assistance of STT effects, meaning that the devices I consider will have both STT and VCMA.

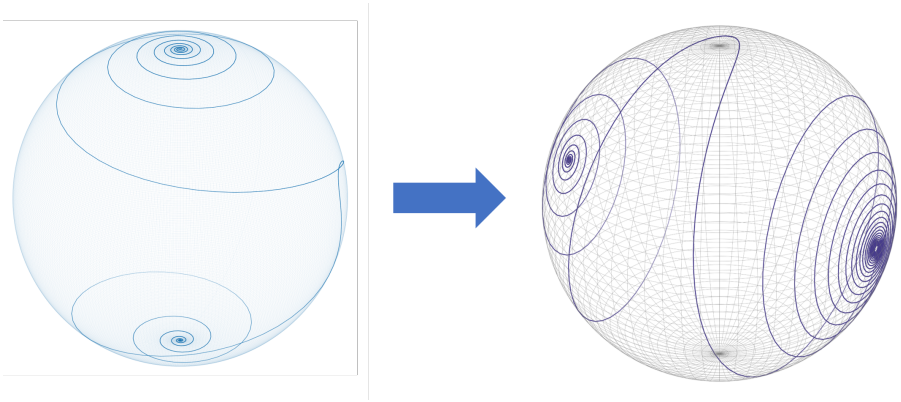

Figure 1.2: Left: A transition from a magnetization direction in the $+z$ direction to the $-z$ direction is plotted on the unit sphere, where the magnetization dynamics rotate around the z-axis. Right: This briefly becomes a rotation around the x-axis under VCMA effects to switch the magnetization direction halfway between $+z$ and $-z$ before switching fully to $-z$ with a STT effect.

The additional effect of VCMA can cause the magnetization direction to lie in the $x - y$ plane instead of the z-axis, which essentially switches the magnet halfway before a STT effect is even applied [13], [14]. This reduces

the dynamic energy required to switch the magnet and can even reduce the switching time of the device. A more in-depth visualization of VCMA from Figure 1.1 can be shown in Figure 1.2.

1.3 Overview

In this thesis, we establish a theoretical background for and focus on the simulation of VCMA device dynamics. In the following subsections I summarize the content of each chapter.

1.3.1 Basic Magnetic Theory

Magnetic theory is both extremely complicated and seldom covered in undergraduate electrical engineering or physics curriculums. I will attempt to provide simple high level explanations of various concepts in magnetism that I had to study and will aid in the understanding of my research project.

1.3.2 Spin Transfer Torque and Voltage Controlled Magnetic Anisotropy

In this section, I will cover research based on first principles calculations of STT and VCMA switching dynamics for bit writes and the properties of STT and VCMA in detail. I will also explain other factors that were modelled building off an understanding of basic magnetic theory.

1.3.3 Results and Methods

The results and methods of my Python simulations of magnetization dynamics will be given and described in detail.

1.3.4 Conclusions and Future Work

I will summarize my conclusions, provide examples of future work, and explain possible extensions of my project that I did not have time to address.

CHAPTER 2

BASIC MAGNETIC THEORY

2.1 Fundamentals of Magnets

The field of magnets is at the forefront of modern research in condensed matter physics, materials science, and electronics. The field and theory continues to change and develop, meaning that many physical effects ranging from simple to complicated are considered as they all can possibly play roles in affecting the behavior of magnets. Furthermore, some effects may be impossible to distinguish from others, and simplified empirical and heuristic models and approximations are often used to reduce the complexity of first principles calculations. In the following subsections, I will explain some concepts that are important to understand my thesis.

2.2 Hysteresis

Figure 2.1 shows an example for a hysteresis curve for a magnet [15]. The loop describes how a magnet's spontaneous magnetization M — the overall magnetization direction of a magnet at any moment in time — acts in response to an imposed magnetic field H or an equivalent field-like effect.

Starting at the origin with a magnet with no magnetization or imposed magnetic field, applying a positive magnetic field increases the magnetization until it reaches the saturation magnetization M_s, which is an intrinsic property of the magnetic material that describes the maximum magnitude of its magnetic state with as many individual magnetic moments pointing in the same direction as possible [16]. Setting H back to zero, however, does not return the magnet back to the origin. Instead, the magnet retains part of its

magnetization and settles on the outer loop to the remanence M_r. The applied magnetic field H must reach a value of the coercivity H_c in the opposite direction in order to reverse its spontaneous magnetization.

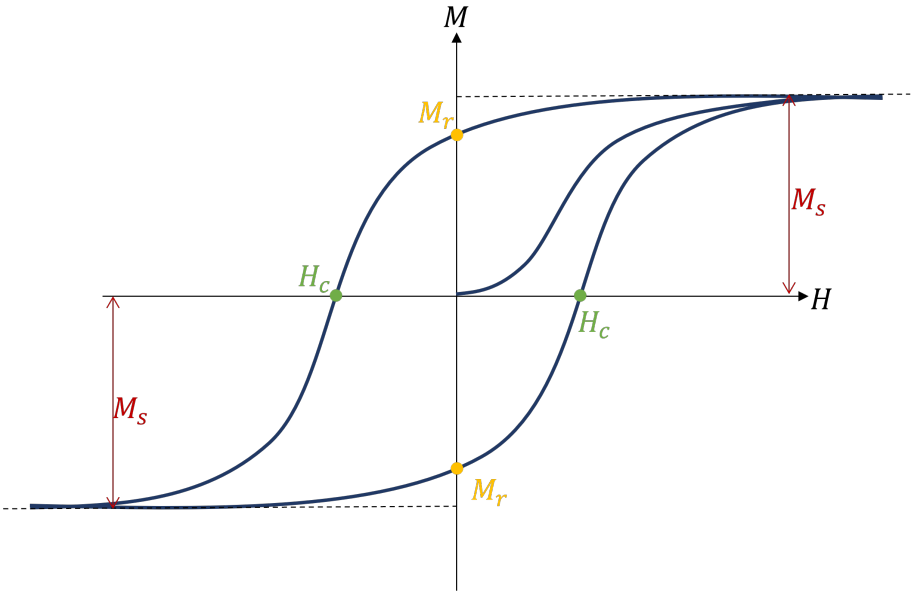

Figure 2.1: An example of a hysteresis curve for a magnet.

H_c and M_r depend on both the material and the physical structure of the material, and magnetic devices can therefore be fabricated while keeping in mind this dependence on physical structure. In particular, an arbitrary division between soft magnets ($H_c \leq$ 1kA/m) and hard magnets ($H_c >$ 100kA/m) is defined to describe the ease of a magnet to switch between its magnetization states [16]. In general, I picked the reference layer of our magnetic devices to be hard magnets, while the free layer is chosen to be of intermediate strength to balance between ease of writing and storage of bit data.

2.3 Anisotropy

The definition of anisotropy is just that magnetic effects and the strength of magnetization are direction dependent [17]. An easy axis for magnetic anisotropy is defined as the direction or directions (if there are more than one) along which the saturation magnetization M_s along the hysteresis curve is the lowest magnitude [16]. This is the direction along which the magneti-

zation prefers to align antiparallelly or parallelly due to it being the direction of lowest energy.

For my research, when I talk about the magnetization transition for magnetic devices between "zero" and "one" bit states, I am talking about choosing a material with a specific anisotropy such that the magnetization switching between the two opposite directions for bit states is along the easy axis of the magnet.

2.3.1 Uniaxial Assumption

In this thesis, I assumed MRAM devices with uniaxial perpendicular magnetic anisotropy (PMA). This means that there is only one easy axis, and that the direction of the easy axis lies perpendicular to the magnet surfaces and parallel to the pathway of current as opposed to in-plane magnetic anisotropy (IMA) magnets with their easy axis direction lying parallel to the magnet surfaces and orthogonal to the current direction. See Figure 2.2 for more clarification. I chose to make a PMA assumption as opposed to an IMA assumption as an analytical expression for PMA magnets can be determined easily [6], and VCMA devices work best with PMA magnets due to their underlying physics [13].

I can write the contribution toward energy density per unit volume of a uniaxial magnet as:

$$E_{uniaxial} = K_1 * \cos^2\theta \tag{2.1}$$

where K_1 is the uniaxial anisotropy constant and θ is the angle between the magnetization direction and the easy axis [6].

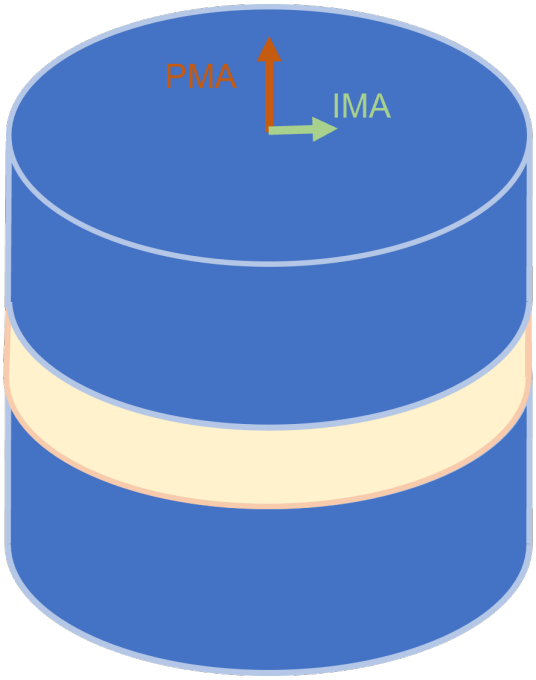

Figure 2.2: Perpendicular Magnetic Anisotropy (PMA) vs In-plane Magnetic Anisotropy (IMA), which lies in the azimuthal plane.

2.3.2 Magnetocrystalline Anisotropy

Anisotropy in general is related to spin orbit coupling interactions with imbalances in the underlying crystal lattice, as orbits of electrons strongly couple with the crystal lattice structure [17]. Magnetocrystalline anisotropy is the anisotropy intrinsic to the original material from this underlying lattice, and values of K_1 are often experimentally determined for specific materials instead of through first principles calculations. Other effects in latter sections can change this lattice slightly and cause anisotropy through extrinsic factors.

2.3.3 Shape Anisotropy and Demagnetizing Field

An applied magnetization induces an internal magnetization that is weaker and opposes the applied magnetization. This effect, known as the demagnetizing field, highly depends on the overall shape of the magnet, and its energy density per unit volume can be written as follows:

$$E_{demag} = -\frac{1}{2}\mathbf{H}_{demag} \cdot \mathbf{M} \tag{2.2}$$

where $\mathbf{H}_{demag}$ is a vector representing the demagnetizing field and $\mathbf{M}$ is the vector representing the magnetization [17]. $\mathbf{H}_{demag}$ can be further broken up into demagnetizing factors $\mathbf{N}_{demag}$ that depend on the shape of the structure, shown in Equation 2.3 [17].

$$\mathbf{H}_{demag} = \mu_0 \mathbf{N}_{demag} \cdot \mathbf{M} \tag{2.3}$$

There are many papers that calculate the demagnetizing factors for different shapes, e.g, ellipsoids and cylinders [18], [19], [20], [21]. For my simulations, I chose to use a cylindrical magnet shape as it is the most likely shape for real devices because of silicon top down fabrication steps. However, demagnetizing factors for cylinders are either too complicated in their usage of elliptic integrals [19], [20]; or not representing the short cylinder shapes we use [18]. I therefore choose to approximate the cylindrical magnet as an oblate ellipsoid [21] in Equation 2.4, a method also used by Kang 2017 [22], where m = diameter/thickness of magnet.

$$\begin{aligned} N_{x,demag} = N_{y,demag} &= \frac{1}{2(m^2-1)}\left[\frac{m^2}{\sqrt{m^2-1}}\sin^{-1}\left(\frac{\sqrt{m^2-1}}{m}\right) - 1\right] \\ N_{z,demag} &= \frac{m^2}{(m^2-1)}\left[1 - \frac{\sin^{-1}\left(\frac{\sqrt{m^2-1}}{m}\right)}{\sqrt{m^2-1}}\right] \end{aligned} \tag{2.4}$$

Equation 2.4 can be rewritten as Equation 2.5.

$$\begin{aligned} N_{x,demag} = N_{y,demag} &= \frac{1 - N_{z,demag}}{2} \\ N_{z,demag} &= \frac{m^2}{(m^2-1)}\left[1 - \frac{\sin^{-1}\left(\frac{\sqrt{m^2-1}}{m}\right)}{\sqrt{m^2-1}}\right] \end{aligned} \tag{2.5}$$

2.3.4 Other Sources of Anisotropy

Some other important influencers of anisotropy are mechanical strain and surface effects.

Because changes in shape and lattice structure can influence the anisotropy,

mechanical strain applied to magnets can induce changes in their anisotropy. MgO, a commonly used insulating material in magnetic devices due to its high spin polarization coefficient, is also a good piezoelectric device, which means it changes its physical dimensions in response to applied electric fields. This could possibly be a contributor toward the VCMA effect [23].

Effects like interactions between orbitals and symmetry breaking that are the most powerful on the surface between interfaces of different materials in a magnetic device can also be important contributors to magnetic anisotropy and magnetic properties of materials, especially if the materials used are very thin layers. The two leading theories behind VCMA to date are both surface changes to anisotropy, also known as interfacial perpendicular magnetic anisotropy (iPMA), on thin films [24], [25].

2.4 Types of Permanent Magnetism

Depending on how individual magnetic moments order themselves in magnets, the overall magnetization direction will be affected. Although the main body of the device is made of ferromagnets, the auxiliary structure can consist of ferrimagnets and antiferromagnets that create environmental secondary effects important to the function of the magnetic device, like a consistent magnetic field or pinning so that the reference layer always remains in the same direction [6], [13]. See Figure 2.3 for a visualization of the different types of permanent magnets.

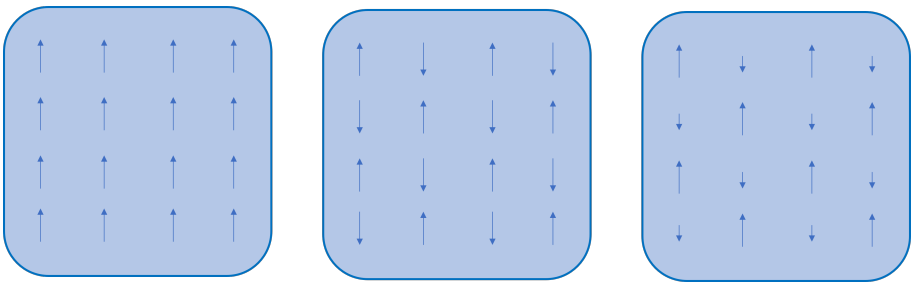

Figure 2.3: From left: Ferromagnetism, Antiferromagnetism, Ferrimagnetism.

2.4.1 Ferromagnetism

In ferromagnetism, all local magnetic moments have a lower energy state when they are pointing in the same direction. There is a strong net magnetization.

2.4.2 Antiferromagnetism

In antiferromagnetism, all local magnetic moments are equal in magnitude and have a lower energy state when they are pointing in opposite directions. There is no net magnetization.

2.4.3 Ferrimagnetism

In ferrimagnetism, local magnetic moments in one direction have a weaker magnetization than the magnetization of magnet moments pointing in the other direction in their lowest energy state. There is a weak net magnetization.

2.5 Spin Orbit Coupling

Electrons and their orbitals undergo an effect known as spin orbit coupling (SOC) where the electron spin angular momentum, S, aligns with their angular momentum from their orbitals, L, in either a parallel or antiparallel fashion [15].

The reason behind this momentum alignment is due to Pauli's exclusion principle, the electron being a fermion and thus needing to occupy antisymmetric states, and the Coulomb interactions between electrons and between electrons and the nucleus of atoms [26].

The exact magnitude of this angular momentum can be calculated from Hund's rules, which are summarized as follows [15]:

1. Maximize the spin angular momentum, S, for the eletrons in an atom.

2. Maximize the orbital angular momentum, L, for the electrons in an atom.

3. Calculate the total angular momentum, J, with the following:

$$J = \begin{cases} L - S & \text{electron shell is less than half full} \\ S & \text{exactly half full} \\ L + S & \text{electron shell is more than half full} \end{cases}$$

For calculating S, the rule is that we first fill all orbitals with $\uparrow$ spin before going back and filling the orbitals with $\downarrow$ spin. Each $\uparrow$ spin contributes $+\frac{1}{2}$ angular momentum while each $\downarrow$ spin contributes $-\frac{1}{2}$ angular momentum.

Calculations for L are slightly more complicated. The orbital type (s, p, d, f) be determined. Then the orbitals are filled with electrons based on the magnetic quantum number m_l and Hund's rules, starting with highest magnetic quantum number first [15], [26]. Table 2.1 contains the spin orbit coupling angular momentum calculations for a d-orbital by listing the values of the occupied orbitals.

Table 2.1: Calculating the total angular momentum J for spin orbit coupling.

# e-	s Values	S (sum)	m_l Values	L (sum)	Half Full?	J
0	N/A	0	N/A	0	$<$	0
1	$\uparrow \times 1$	1/2	2	2	$<$	3/2
2	$\uparrow \times 2$	1	2,1	3	$<$	2
3	$\uparrow \times 3$	3/2	2,1,0	3	$<$	3/2
4	$\uparrow \times 4$	2	2,1,0,-1	2	$<$	0
5	$\uparrow \times 5$	5/2	2,1,0,-1,-2	0	$=$	5/2
6	$\uparrow \times 5, \downarrow \times 1$	2	prev+2	2	$>$	4
7	$\uparrow \times 5, \downarrow \times 2$	3/2	prev+1	3	$>$	9/2
8	$\uparrow \times 5, \downarrow \times 3$	1	prev+0	3	$>$	4
9	$\uparrow \times 5, \downarrow \times 4$	1/2	prev+-1	2	$>$	5/2
10	$\uparrow \times 5, \downarrow \times 5$	0	prev+-2	0	$>$	0

2.6 Exchange Interactions

The exchange interaction is due to electrons minimizing their energy between multiple possible states. These states arise in a multi-orbital system because of wavefunction (wavefunctions correspond to orbitals) overlap from material structure: the overlap of multiple wavefunctions increases the possible space where the electrons can be found and gives electrons more possibilities to find a total antisymmetric wavefunction that has lower energy [15]. The differences in energy level due to these wavefunctions is known as the exchange energy. The exchange interaction is a strong short distance interaction that is responsible for the alignment of magnetic moments in the permanent magnet types from Section 2.4

2.7 Dipole Interactions

The dipole interaction is weaker than the exchange interaction, but can work at a longer distance. It is based off of classic electromagnetic theory related to the Coulomb force.

2.8 Domains

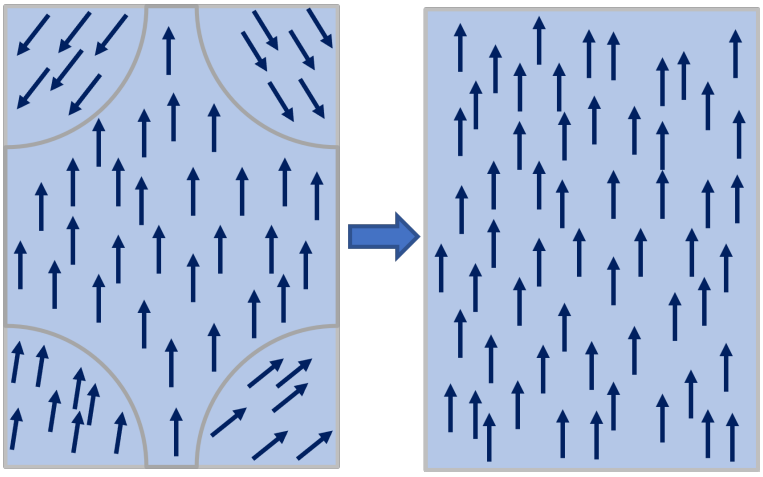

Figure 2.4: In my model, I assumed a monodomain, or macrospin, model for my magnetic device.

Although exchange interactions dominate at smaller scales to create permanent magnets, dipole interactions become greater at larger distances due to dipole interactions between entire domains instead of just between individual spins. Larger magnets have more domains with domains starting to form at the edges of the magnet first.

This complicates my model, so I assumed a macrospin, or monodomain model where the magnet is sufficiently small so that the overall magnetization only considers every individual magnetic moment pointing in the same direction. Devices start to exhibit non-macrospin behavior above 10 nm in diameter [27], but can still be accurate under the macrospin model at larger sizes.

CHAPTER 3

SPIN TRANSFER TORQUE AND VOLTAGE CONTROLLED MAGNETIC ANISOTROPY

3.1 Magnetic Tunnel Junctions

MRAM devices usually consist of many different layers of magnets and other materials called a magnet stack. STT and VCMA devices use a magnetic tunnel junction (MTJ) as the main layers for digital bit storage, consisting of two ferromagnets — one reference hard layer that maintains its magnetization, and one free soft layer that switches its magnetization — and a thin insulator in between. The three layers form a namesake tunnel junction because current passing through the stack tunnels through the insulating layer between the two ferromagnets, retaining a spin polarization according to a spin polarization ratio that is dependent on the material of the insulating layer [6]. See Section 1.2 for details on read and write processes across a MTJ stack.

The most common materials used for the main stack are Fe, CoFe, or CoFeB alloys as the ferromagnet components and MgO as the insulating layer. CoFeB|MgO|CoFeB magnets are standard in MRAM devices and has become the equivalent of transistor technology's Si|SiO_2 devices [13]. MgO as an insulator has very good spin tunneling probability and therefore is the standard for achieving high spin polarization coefficient [28]. Other benefits for CoFeB are its ease in integration for silicon fabrication processes as well as its high TMR ratios, which allow for clearer distinction between "zero" and "one" states [13], [29]. This combination of materials is also good for the VCMA effect as VCMA is caused by interface interactions between thin $3d$ orbital transition metals and nonmagnetic insulators [14].

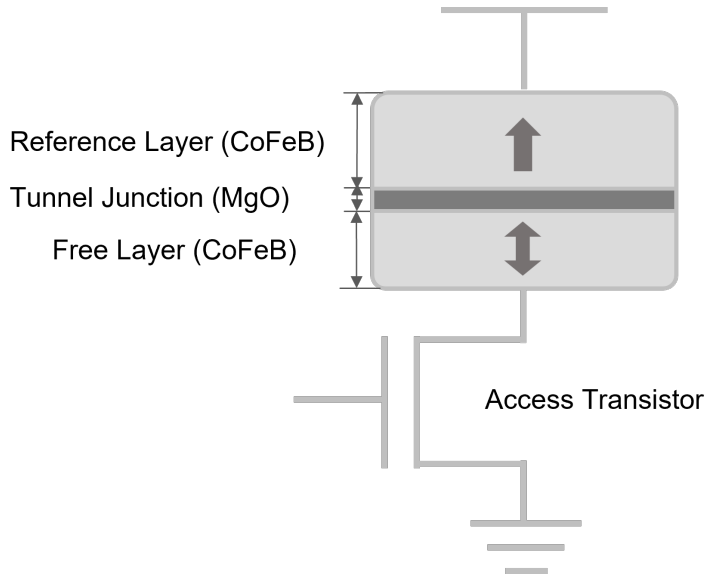

Figure 3.1: The Basic MTJ stack used in my simulations.

3.2 The Landau-Lifshitz-Gilbert-Slonczewski Equation

The time evolution of the magnetization of a magnet can be described by the Landau-Lifshitz-Gilbert-Slonczewski (LLGS) equation in Equation 3.1 [6]. I use this equation to model the switching for the free layer of the MTJ between "zero" and "one" states,

$$\frac{\mathrm{d}\mathbf{M}}{\mathrm{d}t} = -\gamma\mu_0\mathbf{M}\times\mathbf{H}_{eff} + \frac{\alpha}{M_s}\mathbf{M}\times\frac{\mathrm{d}\mathbf{M}}{\mathrm{d}t} - \frac{\gamma a_J}{M_s}\mathbf{M}\times(\mathbf{M}\times\hat{\mathbf{p}}), \qquad (3.1)$$

where M is the magnetization direction, M_s is the saturation magnetization of the ferromagnet, γ is the gyromagnetic ratio, μ_0 is the vacuum permeability, $\mathbf{H}_{eff}$ is the effective magnetic field, α is the Gilbert damping constant, $\hat{\mathbf{p}}$ is the unit vector which describes the direction of the spin within the spin current, and a_J represents the strength of the STT spin torque.

The first term on the right hand side of the equation describes a precessional torque that causes spinning of the magnetization around the effective magnetic field, $\mathbf{H}_{eff}$. The second term on the right hand side is the damping term, which is a frictional force that causes the magnetization to align back to the effective magnetic field's direction. The third term represents the motion induced by the spin polarized transfer current from STT and resists or

assists the second damping term to cause the actual switching of the magnet. A graphical representation of these torques can be seen in Figure 3.2.

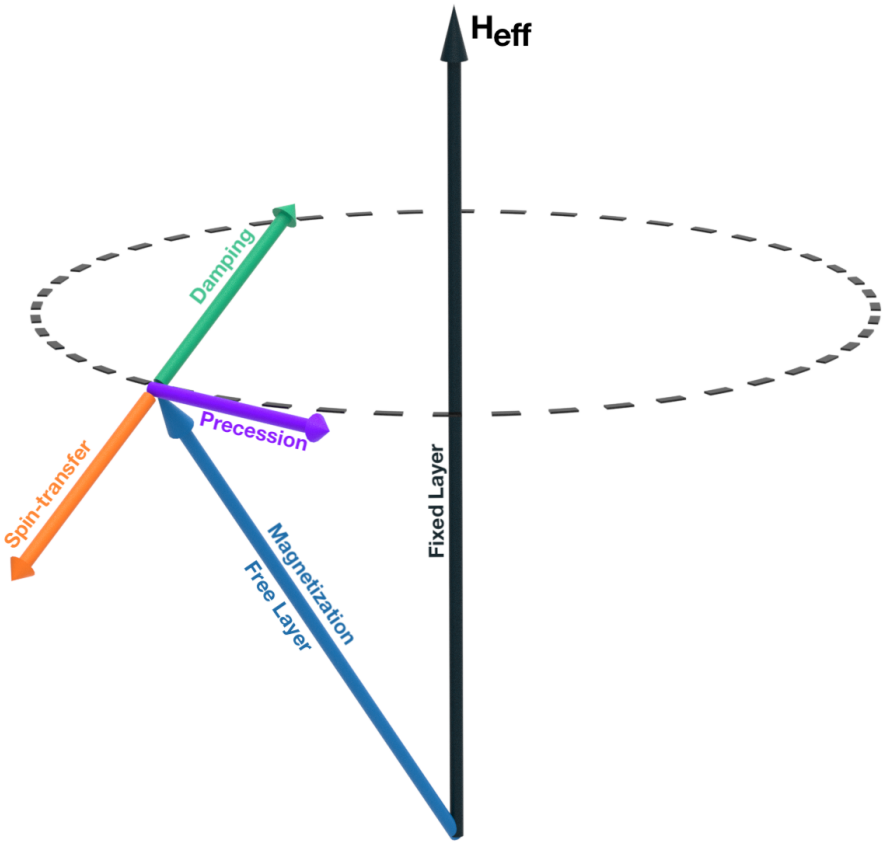

Figure 3.2: Modified from [6]. The forces acting on the magnet's magnetization according to the LLGS equation.

3.2.1 Derivation of the Explicit Form

I derive the explicit form of the LLGS equation from the implicit form in Equation 3.1 for a PMA monodomain magnet with STT torque in cartesian coordinates with no field like torque and no thermal effects. The explicit form is necessary to solve the LLGS on a computer. I first start with the LLGS in Equation 3.1, and follow the methods described by Ament [30].
I follow by expanding out the a_J term. The units are verified with Sebastian Ament's previous paper [30].

$$\frac{\mathrm{d}\mathbf{M}}{\mathrm{d}t} = -\gamma\mu_0\mathbf{M}\times\mathbf{H}_{eff} + \frac{\alpha}{M_s}\mathbf{M}\times\frac{\mathrm{d}\mathbf{M}}{\mathrm{d}t} - \frac{\gamma\hbar\eta I}{2eM_s^2(\mathrm{Vol})}\mathbf{M}\times(\mathbf{M}\times\hat{\mathbf{p}}) \quad (3.2)$$

In Equation 3.2, $\hbar$ is the reduced Planck constant, η is the spin polarization coefficient, e is the charge of an electron, I is the magnitude of the current flowing through the MTJ, and Vol is the volume of the free layer ferromagnet. Following Appendix A in Ament's paper [30], I divide both sides of the equation by $\gamma\mu_0 M_s^2$.

$$\frac{\frac{\mathrm{d}\mathbf{M}}{\mathrm{d}t}}{\gamma\mu_0 M_s^2} = \frac{-\mathbf{M}\times\mathbf{H}_{eff}}{M_s^2} + \frac{\alpha}{\gamma\mu_0 M_s^3}\mathbf{M}\times\frac{\mathrm{d}\mathbf{M}}{\mathrm{d}t} - \frac{\hbar\eta I}{2e\mu_0 M_s^4(\mathrm{Vol})}\mathbf{M}\times(\mathbf{M}\times\hat{\mathbf{p}}) \quad (3.3)$$

I normalize $\mathbf{M}$ and $\mathbf{H}_{eff}$ by dividing by substituting $\mathbf{m}$ for $\frac{\mathbf{M}}{M_s}$ and $\mathbf{h}_{eff}$ for $\frac{\mathbf{H}_{eff}}{M_s}$. $\mathbf{m}$ is now a vector with a magnitude of 1.

$$\frac{\frac{\mathrm{d}\mathbf{m}}{\mathrm{d}t}}{\gamma\mu_0 M_s} = -\mathbf{m}\times\mathbf{h}_{eff} + \frac{\alpha}{\gamma\mu_0 M_s}\mathbf{m}\times\frac{\mathrm{d}\mathbf{m}}{\mathrm{d}t} - \frac{\hbar\eta I}{2e\mu_0 M_s^2(\mathrm{Vol})}\mathbf{m}\times(\mathbf{m}\times\hat{\mathbf{p}}) \quad (3.4)$$

I divide the current, I by a factor $\frac{2e\mu_0 M_s^2(\mathrm{Vol})}{\hbar\eta}$, and combine this into the vector i in place of $\hat{\mathbf{p}}$, and divide the time by $\gamma\mu_0 M_s$, combining this into the time term τ. After substituting these new values, I have the following, which is the normalized LLGS equation.

$$\frac{\mathrm{d}\mathbf{m}}{\mathrm{d}\tau} = -\mathbf{m}\times\mathbf{h}_{eff} + \alpha\,\mathbf{m}\times\frac{\mathrm{d}\mathbf{m}}{\mathrm{d}\tau} - \mathbf{m}\times(\mathbf{m}\times\mathbf{i}) \quad (3.5)$$

The goal of this next segment is to derive the explicit form of the LLGS equation by removing the $\mathbf{m}\times\frac{\mathrm{d}\mathbf{m}}{\mathrm{d}\tau}$ term on the right hand side. To do this, I apply a cross product with $\mathbf{m}$ on both sides.

$$\mathbf{m}\times\frac{\mathrm{d}\mathbf{m}}{\mathrm{d}\tau} = -\mathbf{m}\times(\mathbf{m}\times\mathbf{h}_{eff}) + \alpha\,\mathbf{m}\times(\mathbf{m}\times\frac{\mathrm{d}\mathbf{m}}{\mathrm{d}\tau}) - \mathbf{m}\times(\mathbf{m}\times(\mathbf{m}\times\mathbf{i})) \quad (3.6)$$

I simplify the previous equation with the following property,

$$\mathbf{A} \times (\mathbf{B} \times \mathbf{C}) \;=\; \mathbf{B}(\mathbf{A} \cdot \mathbf{C}) - \mathbf{C}(\mathbf{A} \cdot \mathbf{B}),$$

where $\mathbf{A}$, $\mathbf{B}$, $\mathbf{C}$ are vectors. This results in the following two simplifications:

$$\begin{aligned} &\alpha\, \mathbf{m} \times (\mathbf{m} \times \frac{\mathrm{d}\mathbf{m}}{\mathrm{d}\tau}) \\ &= \alpha\, (\mathbf{m}(\mathbf{m} \cdot \frac{\mathrm{d}\mathbf{m}}{\mathrm{d}\tau}) - \frac{\mathrm{d}\mathbf{m}}{\mathrm{d}\tau}(\mathbf{m} \cdot \mathbf{m})) \end{aligned}$$

For a fixed length vector (constant magnitude), $(\mathbf{m} \cdot \frac{\mathrm{d}\mathbf{m}}{\mathrm{d}\tau}) \;=\; 0$. Also, since I already defined $\mathbf{m}$ to have magnitude 1, $(\mathbf{m} \cdot \mathbf{m}) \;= \|\mathbf{m}^2\| = \; 1$

$$\begin{aligned} &= \alpha\, (0 - \frac{\mathrm{d}\mathbf{m}}{\mathrm{d}\tau} 1) \\ \alpha\, \mathbf{m} \times (\mathbf{m} \times \frac{\mathrm{d}\mathbf{m}}{\mathrm{d}\tau}) \;&=\; -\alpha \frac{\mathrm{d}\mathbf{m}}{\mathrm{d}\tau} \end{aligned} \tag{3.7}$$

I now shift the focus to the $\mathbf{m} \times (\mathbf{m} \times (\mathbf{m} \times \mathbf{i})$ term.

$$\begin{aligned} &\mathbf{m} \times (\mathbf{m} \times (\mathbf{m} \times \mathbf{i}) \\ &= \mathbf{m}(\mathbf{m} \cdot (\mathbf{m} \times \mathbf{i})) - (\mathbf{m} \times \mathbf{i})(\mathbf{m} \cdot \mathbf{m}) \end{aligned}$$

$\mathbf{m} \times \mathbf{i}$ is orthogonal to both $\mathbf{m}$ and $\mathbf{i}$. Since $\mathbf{m}$ is orthogonal to $\mathbf{m} \times \mathbf{i}$, $\mathbf{m} \cdot (\mathbf{m} \times \mathbf{i}) \;=\; 0$. $\mathbf{m} \cdot \mathbf{m} \;=\; 1$ still holds.

$$\begin{aligned} &= 0 - (\mathbf{m} \times \mathbf{i}) * 1 \\ &\mathbf{m} \times (\mathbf{m} \times (\mathbf{m} \times \mathbf{i}) = -\mathbf{m} \times \mathbf{i} \end{aligned} \tag{3.8}$$

I substitute Equations 3.7 and 3.8 into Equation 3.6.

$$\mathbf{m} \times \frac{\mathrm{d}\mathbf{m}}{\mathrm{d}\tau} \;=\; -\mathbf{m} \times (\mathbf{m} \times \mathbf{h}_{eff}) - \alpha \frac{\mathrm{d}\mathbf{m}}{\mathrm{d}\tau} + \mathbf{m} \times \mathbf{i} \tag{3.9}$$

I substitute Equation 3.9 into Equation 3.5 on the right hand side.

$$\frac{\mathrm{d}\mathbf{m}}{\mathrm{d}\tau} = -\mathbf{m}\times\mathbf{h}_{eff} + \alpha\left(-\mathbf{m}\times(\mathbf{m}\times\mathbf{h}_{eff}) - \alpha\frac{\mathrm{d}\mathbf{m}}{\mathrm{d}\tau} + \mathbf{m}\times\mathbf{i}\right) - \mathbf{m}\times(\mathbf{m}\times\mathbf{i})$$

$$(1+\alpha^2)\frac{\mathrm{d}\mathbf{m}}{\mathrm{d}\tau} = -\mathbf{m}\times\mathbf{h}_{eff} + \alpha\left(-\mathbf{m}\times(\mathbf{m}\times\mathbf{h}_{eff}) + \mathbf{m}\times\mathbf{i}\right) - \mathbf{m}\times(\mathbf{m}\times\mathbf{i})$$

$$\boxed{\frac{\mathrm{d}\mathbf{m}}{\mathrm{d}\tau} = \frac{1}{1+\alpha^2}\left[-\alpha\,\mathbf{m}\times(\mathbf{m}\times\mathbf{h}_{eff}) - \mathbf{m}\times\mathbf{h}_{eff} + \alpha\,\mathbf{m}\times\mathbf{i} - \mathbf{m}\times(\mathbf{m}\times\mathbf{i})\right]} \tag{3.10}$$

3.3 The Energy Barrier

The energy barrier is the amount of energy the magnetization must overcome to switch the MTJ system from a parallel (P) to anti-parallel (AP) state and vice versa in terms of the relationship between the reference layer magnetization direction and the free layer magnetization direction. This barrier value can be calculated by finding the E_{max} - E_{min} of the total energy, which is visualized in Figure 3.3.

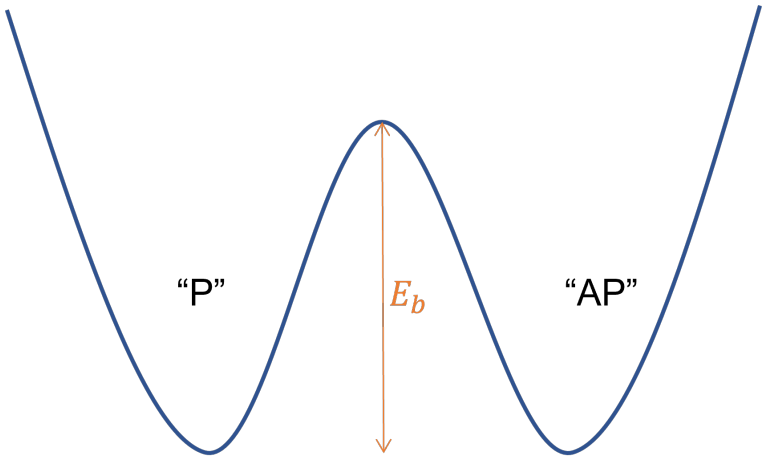

Figure 3.3: The energy barrier between parallel (P) and anti-parallel (AP) magnetization states. The energy barrier must be overcome to switch the magnetization fully to the correct orientation.

An equation for the total energy can be determined by a sum of the uniaxial anisotropy energy from Equation 2.1 and the demagnetizing energy from Equation 2.2, as well as including the energy from an applied magnetic field and energy from thermal effects [30]. Ignoring stochastic thermal effects, the total energy can be written as:

$$\begin{aligned} E_{total} &= \text{Vol} * (E_{app} + E_{uniaxial} + E_{demag}) \\ &= \text{Vol} * \left[\mu_0(\mathbf{H}_{app} \cdot \mathbf{M}) + K_1 * \cos^2\theta - \frac{1}{2}\mu_0(\mathbf{N}_{demag} \cdot \mathbf{M})\mathbf{M} \right], \end{aligned} \tag{3.11}$$

where E_{app} is the energy of the externally applied magnetic field, H_{app} is the externally applied magnetic field, Vol is the volume of the free layer ferromagnet, and the rest can be determined from Equations 2.1 and 2.2. Only the $E_{uniaxial}$ and E_{demag} energies change in terms of energy magnitude, so only these terms are used to determine E_{max} - E_{min}. I assumed a sufficiently thin magnet such that $N_{demag,z} \gg N_{demag,x} = N_{demag,y}$, allowing me to write the energy barrier as shown in Equation 3.12.

$$\begin{aligned} E_b &= E_{max} - E_{min} \\ &= \text{Vol} * (K_1 - \frac{1}{2}\mu_0 M_s^2) \end{aligned} \tag{3.12}$$

3.3.1 Magnetization Lifetime vs Writing Effort

The energy barrier is unique to the MRAM device structure chosen, and provides a tradeoff between writing energy and the stability of the magnet. The magnetization of a MRAM device can spontaneously switch under thermal effects with certain probabilities unintentionally — magnets have a magnetization lifetime within which they are expected to be reliable. A higher energy barrier will lower the probabilities of switching and increase this lifetime, but will also mean that larger energies are required to write data to the magnet and intentionally switch it. Therefore, energy barriers of around $30 * k_bT$ to $80 * k_bT$ are usually desired depending on the application (shorter term fast switching memories, or longer term storage memories) and the MTJ structure, where k_b is the Boltzmann constant and T is the temperature in Kelvin [13].

3.4 Effective Magnetic Field

The precessional first term of the LLGS equation (Equation 3.1) contains a reference to an effective magnetic field. This field consists of a total sum that is related to the E_{total} in Equation 3.11. This total field can be written as:

$$\mathbf{H}_{eff} = \mathbf{H}_{app} + \mathbf{H}_{uniaxial} + \mathbf{H}_{demag} + \mathbf{H}_{thermal}, \tag{3.13}$$

where it is the sum of the external applied magnetic field, uniaxial anisotropy magnetic field, demagnetizing field, and thermal field, respectively. It can be derived from Equation 3.14 [6].

$$\mathbf{H}_{eff} = -\frac{1}{\mu_0 \mathrm{Vol}} \frac{\partial E_{total}(\theta)}{\partial \mathbf{M}} \tag{3.14}$$

3.5 Thermal Effects

The $\mathbf{H}_{thermal}$ term of the effective magnetic field must be considered for accurate results. This can be modelled as a Gaussian function with a standard deviation shown in Equation 3.15 under the Wiener process where Δt is the time step of the computer simulation [30], but was not included in my simulations as I simulated qualitative deterministic results.

$$\sigma_{stdv} = \sqrt{\frac{2\alpha k_b T \Delta t}{\gamma \mu_0^2 M_s \mathrm{Vol}}} \tag{3.15}$$

3.6 The Critical Current

The critical current, I_{c0}, is the current necessary to switch a magnet's magnetization and overcome the energy barrier under deterministic conditions. For a PMA magnet with our assumptions, it can be derived analytically and is shown in Equation 3.16 [6].

$$I_{c0} = \frac{4eE_b\alpha}{\hbar\eta} \tag{3.16}$$

3.7 The Voltage Controlled Magnetic Anisotropy Modification

Voltage controlled magnetic anisotropy (VCMA) is a method to control the magnetic anisotropy of the free layer by applying a voltage that induces an electric field. This electric field alters properties on the interfaces of the ferromagnet and insulator layers to create an interfacial perpendicular magnetic anisotropy (iPMA). This effect is often applied such that the magnetization direction of the free layer is reduced along the same axis as the reference layer, creating an effective energy barrier reduction [22]. When the bias voltage V_b across the MTJ is equal to zero, the MRAM device behaves as a normal device with energy barrier of E_{b0}. The different regimes of E_b for V_b compared to zero and to the VCMA critical voltage V_c for the magnet states is summarized in Equation 3.17 and is demonstrated in Figure 3.4.

$$E_b \begin{cases} > E_{b0} & V_b < 0 \\ = E_{b0} & V_b = 0 \\ < E_{b0} & 0 < V_b < V_c \\ \leq 0 & V_c < V_b \end{cases} \tag{3.17}$$

Three main types of VCMA are used to control magnet behavior: precessional VCMA switching, thermally activated switching, and STT assisted VCMA switching. In this paper I explored STT assisted VCMA switching and its properties. A comparison can be shown in Figure 3.5.

For precessional VCMA switching, $V_b > V_c$, removes the energy barrier. An external magnetic field is then applied in the in-plane direction, causing precessional motion and turning the perpendicular magnetic anisotropy (PMA) magnet into an in-plane magnetic anisotropy (IMA) magnet. If timed correctly, the magnet can then deterministically switch between its two write states [22]. In practical applications this is hard to time due to the randomness of thermal noise, so this method is unlikely to work.

In thermally activated VCMA switching, the VCMA effect is only used to reduce the energy barrier partway by applying $V_b < V_c$. This allows a magnet to switch under another effect like STT with less energy and with less critical

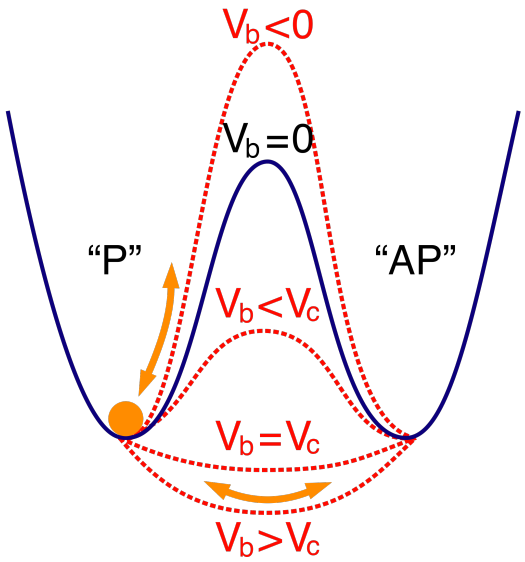

Figure 3.4: Modified from [22]. Applying a bias voltage V_b across the MTJ stack causes varying effects to the energy barrier between parallel (P) and anti-parallel (AP) states of the magnet, making it easier or harder to switch.

current than without the VCMA effect.

The method that I chose to simulate was STT assisted VCMA switching, which was touted as the most energy efficient by Kang in his paper [22]. In this method, the energy barrier is fully reduced and the magnetization of the free layer is moved to an in-plane orientation by the VCMA effect. A secondary STT pulse is applied after the original voltage pulse that induces the VCMA effect to create a STT effect that fully transitions the magnet to the other desired state.

An important concern to note is that the VCMA and STT effects are competing effects when voltage is used to control both in a two terminal device. While positive voltages may not pose a problem and will cause STT and VCMA to work together in switching the magnet (e.g, switching P $\rightarrow$ AP), negative voltages create conflict. A negative voltage creates a higher energy barrier in the case of VCMA, while a negative voltage is necessary to produce a spin current in the opposite direction for the STT effect, which is the only

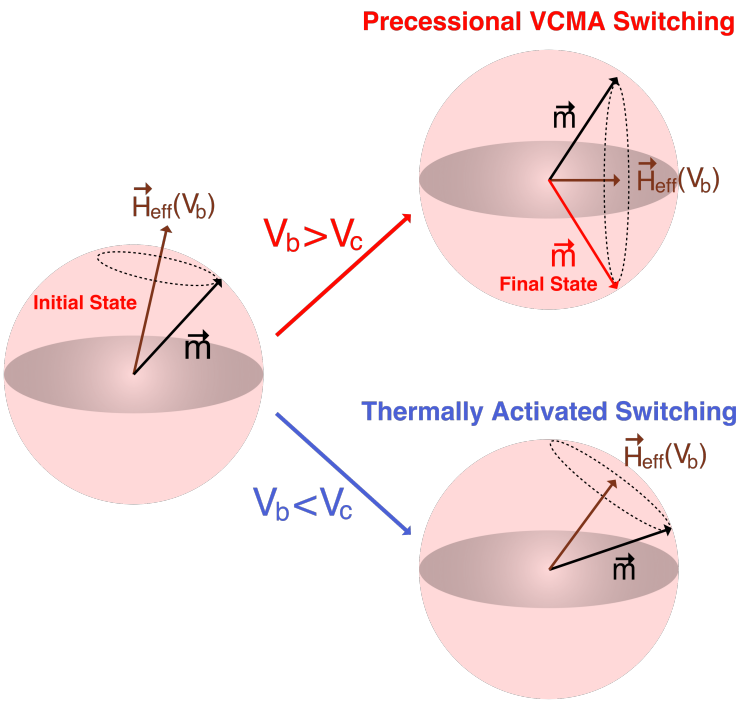

Figure 3.5: Modified from [22]. A visualization of how the anisotropy changes under the VCMA effect for different regimes.

way the magnet can switch in the opposite direction (e.g, switching AP $\rightarrow$ P). This causes a significant imbalance in switching behavior in terms of the direction of switching, and a solution involving an external magnetic field in the perpendicular direction has been proposed to handle this issue [13].

3.7.1 Underlying Physics

The physics behind VCMA is still in the process of being understood, and it is likely that many effects are jointly responsible for the VCMA effect. There are two main theories that both have experimental backing: an orbital based theory [25] and a Rashba effect based theory [24]. Two other possible effects that change magnetic anisotropy due to voltage include a theory based on the quadrupole interaction [31] and a theory based on the piezoelectric effect of MgO [23].

For the orbital based theory behind the VCMA effect, electric field has screening depths in metals, and thus this effect can only occur in thin films and

create an iPMA. At the interfaces between ferromagnets and the oxide insulator, electrons are moved out of their perpendicular orbitals and into in-plane orbitals due to the electric field. From spin orbit coupling, this also means that the angular moment of the electrons becomes aligned with the orbitals, and the overall anisotropy in the perpendicular direction is reduced. A follow-up paper measures the charge and spin distributions at the surfaces of the metal layers to further observe this orbital effect's impact [32]. The anisotropy change is taken to be linearly proportional with the applied electric field [25].

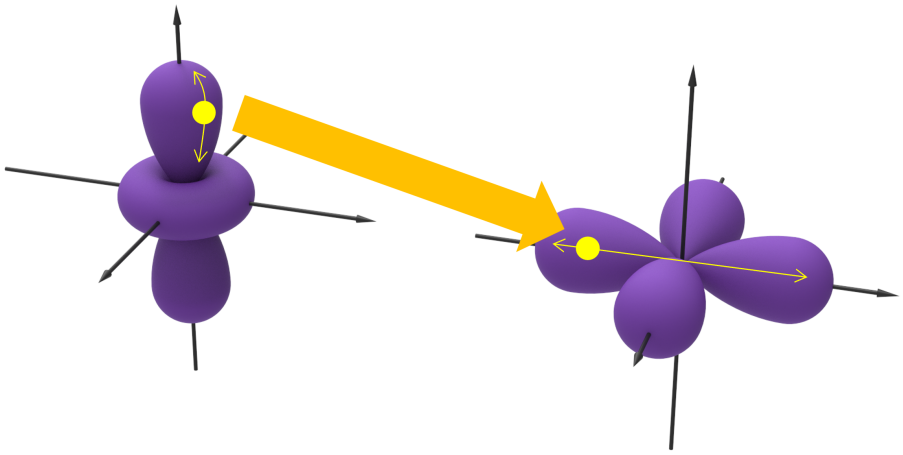

Figure 3.6: A demonstration of an electron changing from a perpendicular orbital to an in-plane orbital, with its angular momentum changing directions along with the transition.

The Rashba effect is an effect often used in spin orbit torque (SOT) devices and is due to the symmetry breaking of the overall stack structure in the perpendicular direction. The asymmetry causes a net magnetic field and a large internal electric field when an electric field is applied by means of a voltage, which then causes spin splitting of the band structure. The spin splitting along with spin orbit coupling creates a reduced anisotropy along the same axis as the reference layer [13], [24]. The anisotropy reduction is related to the total field, which is a sum of the external electric field applied as well as the induced internal electric field.

A large internal field was assumed, resulting in the Taylor approximation in Equation 3.18 for the case of large asymmetry and $E_{internal} \gg E_{applied}$ [13].

The dependence of the magnetic anisotropy on the external field becomes approximately linear.

$$\begin{aligned} E_{total} &= (E_{internal} + E_{applied})^2 \\ &= E_{internal}^2 \left(1 + \frac{E_{applied}}{E_{internal}}\right)^2 \\ &\approx E_{internal}^2 \left(1 + \frac{2E_{applied}}{E_{internal}}\right) \\ &= E_{internal}^2 + 2E_{internal}E_{applied} \end{aligned} \tag{3.18}$$

Since the anisotropy reduction by the electric field is an approximately linear effect, taking the Taylor expansion of this energy barrier reducing effect means only the first order terms need to be considered for a model. The VCMA modification of the uniaxial anisotropy is described in Equation 3.19 [13], [22].

$$K_1(V_b) = K_1(0) - \frac{\xi V_b}{t_{ox} t_{free}} \tag{3.19}$$

Equation 3.19 has ξ as the VCMA coefficient, which is typically a device parameter on the order of 30 – 60 fJ / V m. V_b is the applied bias voltage across the MTJ, t_{ox} is the thickness of the oxide MgO layer, and t_{free} is the thickness of the free magnet layer. The intuition behind this is that V_b/t_{ox} is the applied electric field across the dielectric, while a division by t_{free} occurs because the VCMA effect is an interfacial effect.

3.7.2 Modification to the Energy Barrier

Equation 3.12 is modified by the VCMA effect to produce Equation 3.20. This energy barrier is dynamic and changes in the simulations based on the applied voltage values.

$$\begin{aligned} E_b(V_b) &= E_{max} - E_{min} \\ &= \text{Vol} * (K_1 - \frac{\xi V_b}{t_{ox} t_{free}} - \frac{1}{2}\mu_0 M_s^2) \end{aligned} \tag{3.20}$$

3.7.3 Modifications to the Critical Current

The critical retains its expression described in Equation 3.16, but it must be noted that the energy barrier E_b is now dependent on the applied voltage; as such the critical current can changed during simulation with the VCMA bias voltage.

In addition to this effect, VCMA also has a significant impact on the magnetization direction for values of $V_b > V_c$, bringing the magnetization direction from perpendicular to in-plane. I now derive an angular dependent critical current. I start with analytical calculations of the expected magnetization switching time from Huanlong for a PMA magnet, with the definitions of x_f, x_i, i, H_k and τ_D preceding the initial equation [6].

$$\begin{aligned} x_f &\equiv \tan\left(\frac{\theta_f}{2}\right) \\ x_i &\equiv \tan\left(\frac{\theta_i}{2}\right) \\ H_k &\equiv \frac{2E_b}{\mu_0 M_s \mathrm{Vol}} \\ \tau_D &\equiv \left(\frac{1+\alpha^2}{\alpha\gamma\mu_0 H_k}\right) \\ i &\equiv \frac{I}{I_{c0}} - \frac{H_{app}}{H_k} \\ (i-1)\frac{\tau}{\tau_D} &= \ln\left(\frac{x_f}{x_i}\right) - \frac{1}{i+1}\ln\left(\frac{\frac{i-1}{i+1}+x_f^2}{\frac{i-1}{i+1}+x_i^2}\right) \end{aligned} \tag{3.21}$$

Equation 3.21 describes the switching time τ for an initial angle θ_i to a final angle θ_f with respect to the perpendicular axis in spherical coordinates. tau_D is a time scaling parameter; i represents a critical current ratio where I is the magnitude of the applied spin current, I_{c0} is the critical current, H_{app} is an applied external magnetic field, and H_k represents a zero temperature coercive field [6].

I target values for $I < I_{c0}$, meaning $i < 1$, to find initial angles where the current can still switch under the critical current to derive the new angular dependent critical current. The limiting condition for finding this angular

dependent critical current is for $\frac{\tau}{\tau_D}$ to be infinite or undefined for a particular current. This means that switching is not possible in that regime. The conditions for an undefined value of $\frac{\tau}{\tau_D}$ happens first when the argument of the second natural log on the right side of Equation 3.21 becomes less than zero. I solve with this in mind.

$$\begin{aligned} \ln\left(\frac{\frac{i-1}{i+1}+x_f^2}{\frac{i-1}{i+1}+x_i^2}\right) &= \text{undef} \\ \frac{\frac{i-1}{i+1}+x_f^2}{\frac{i-1}{i+1}+x_i^2} &< 0 \end{aligned} \tag{3.22}$$

I assume the magnetization travels from a $\theta_i < \pi/2$ to a $\theta_f > \pi/2$ state. (The final result can easily be negated to produce the case of switching in the opposite direction). This means that the condition $x_f^2 > x_i^2 > 0$ will always be true. The only possibility for the fraction in Equation 3.22 to be less than zero is for the denominator to be less than zero, while the numerator remains positive from the $x_f^2 > x_i^2$ condition. In the last step of Equation 3.23, I flip the sign of the inequality to change the equation to represent all the values where the equation is defined instead of for all the values where the equation is undefined. This will give the angular dependent critical current in Equation 3.23.

$$\begin{aligned} \frac{i-1}{i+1}+x_i^2 &< 0 \\ i-1+x_i^2(i+1) &< 0 \\ i(1+x_i^2)-1(1-x_i^2) &< 0 \\ \boxed{i > \frac{1-x_i^2}{1+x_i^2}} & \end{aligned} \tag{3.23}$$

3.7.4 The Critical Voltage

Equation 3.20 can be solved for the value of the bias voltage V_b such that $E_b = 0$. This value is the value known as the critical voltage V_c, with A being the cross sectional area of the free layer.

$$
\begin{aligned}
E_b(V_b) &= 0 \\
&= \mathrm{Vol} * (K_1 - \frac{\xi V_c}{t_{ox} t_{free}} - \frac{1}{2}\mu_0 M_s^2) \\
\frac{\mathrm{Vol}\ \xi V_c}{t_{ox} t_{free}} &= E_b(0) \\
V_c &= \frac{t_{ox} E_b(0)}{\xi A}
\end{aligned}
\tag{3.24}
$$

3.7.5 Dielectric Breakdown

Applying large voltage across MTJ devices can cause dielectric breakdown of the MgO layers [33], [34]. The voltage and electric field values I used in my simulation exceed breakdown levels for my devices, meaning more work must be done to ensure breakdown of real experiments does not occur. Although my values may not work on real device, VCMA switching has been demonstrated in experimental devices with success below breakdown voltages [35].

CHAPTER 4

RESULTS AND METHODS

4.1 Description of Simulated Magnetic Tunnel Junction

For my simulations, I used a PMA magnet with a CoFeB|MgO|CoFeB stack. The perpendicular direction is in the z-direction, with just the free layer shown in Figure 4.1. In particular, I wanted to observe the effects of VCMA and STT with more control, so I chose a three-terminal device where the voltage is applied across the main stack and a current is passed through an effect similar to SOT as shown in Figure 1.1.

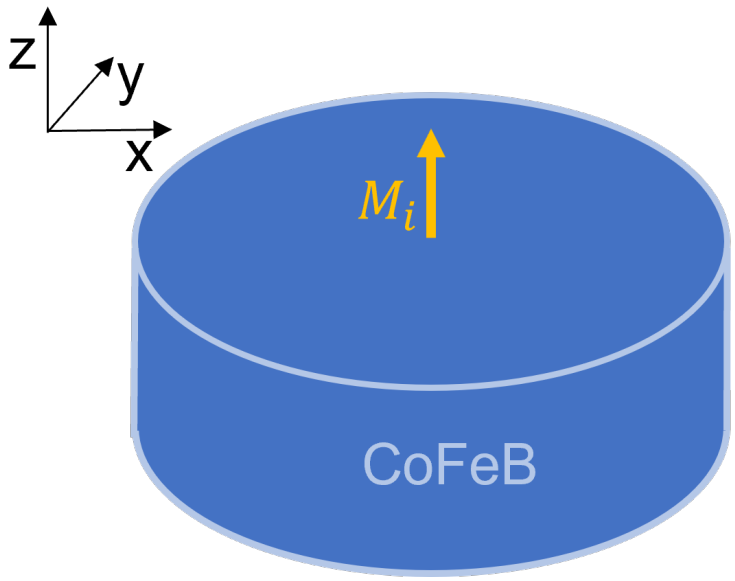

Figure 4.1: The free layer of my PMA magnet, and the corresponding coordinate directions in the top left.

In terms of specific parameter values, I chose numbers from the same stack that Kang uses, but modified so that some calculations match [22]. Some

differences are that instead of using a two-terminal device like in their paper, I use a three terminal device and decouple the voltage and current by ignoring the resistance models. I never apply an external magnetic field to my experiments, and I use a larger magnet area to reach the desired 40 k_bT stability factor. I also use a different definition for the gyromagnetic ratio: $\gamma = \gamma_{Kang}/\mu_0$. The parameter values I use are in Table 4.1.

Table 4.1: The experimental parameters used in my simulations.

Parameter	Description	Value
γ	Gyromagnetic Ratio	1.76 * 10^{11} rad/s T
μ_0	Vacuum Permeability	1.257 * 10^{-6} H/m
k_b	Boltzmann Constant	1.381 * 10^{-23} J/K
e	Elementary Charge	1.602 * 10^{-19} C
$\hbar$	Reduced Planck Constant	1.055 * 10^{-34} J s
K_i	Interfacial PMA = $K_1 * t_f$	$3.2 * 10^{-4}$ J/m^2
M_s	Saturation Magnetization	6.25 * 10^5 A/m
ξ	VCMA Coefficient	60 fJ/V m
d	MTJ Diameter	57.63 nm
t_{ox}	MgO Oxide Thickness	1.4 nm
t_f	CoFeB Free Layer Thickness	1.1 nm
α	Gilbert Damping Constant	0.05
η	Spin Polarization Coefficient	0.58
T	Temperature	300 K
$\Delta(0)$	Thermal Stability Factor = E_b/k_bT	40

4.2 Python: Magnetization Time Evolution Model

For my magnetization time evolution model, I used a numerical method approach to solve the LLGS differential equation. Euler's method for solving the LLGS equation is not accurate under thermal effects, and therefore should not be used. Any Runge-Kutta methods or the midpoint method will produce more accurate results. I used Equation 3.10 and implemented a numerical method solver using Heun's method, which is similar to a two=stage Runge-Kutta method, for solving ordinary differential equations to solve the magnetization time evolution in Cartesian coordinates. The steps for Heun's method are as follows:

1. Find the initial value for the magnetization. I use an initial angle θ_0:

$$\theta_0 = \sqrt{\frac{k_b T}{2E_b(0)}}$$

2. Make an intermediate estimate for the value $\tilde{\mathbf{m}}_{i+1}$ at the endpoint of this time step using:

$$\tilde{\mathbf{m}}_{i+1} = \mathbf{m}_i + t_{step}\frac{\mathrm{d}\mathbf{m}_i}{\mathrm{d}t}$$

with time step t_{step}, and the subscript i denoting the iteration.

3. Make a final, more accurate estimation for the value $\mathbf{m}_{i+1}$ at the endpoint of this time step by averaging the slope from the beginning of the this time step with the slope from "the end (using the intermediate value)" of this time step with:

$$\mathbf{m}_{i+1} = \mathbf{m}_i + \frac{t_{step}}{2}\left(\frac{\mathrm{d}\mathbf{m}_i}{\mathrm{d}t} + \frac{\mathrm{d}\tilde{\mathbf{m}}_i}{\mathrm{d}t}\right)$$

4.3 Results

For my simulations, I attempted to replicate the work done by Kang [22] and the three different types of VCMA effects mentioned in Section 3.7 . The purpose was to gain a better understanding of the different operating regimes for VCMA and to decouple the VCMA and STT effects across the MTJ so that the effects could be understood separately. For each type of simulation, I include the voltage and current pulses used to drive magnetization changes in the single-cell magnetic memory device and plot their magnetization state transitions over time.

4.3.1 Voltage Only Control

Under voltage only control of the VCMA device, I apply a $V_b = 2\text{V} > V_c$. The voltage pulse is shown in Figure 4.2, while the anisotropy conversion

from PMA to IMA is demonstrated in Figures 4.3 – 4.6. This shows that a bias voltage can change the energy barrier and even move the magnet to $z = 0$, but cannot create fully switching behavior.

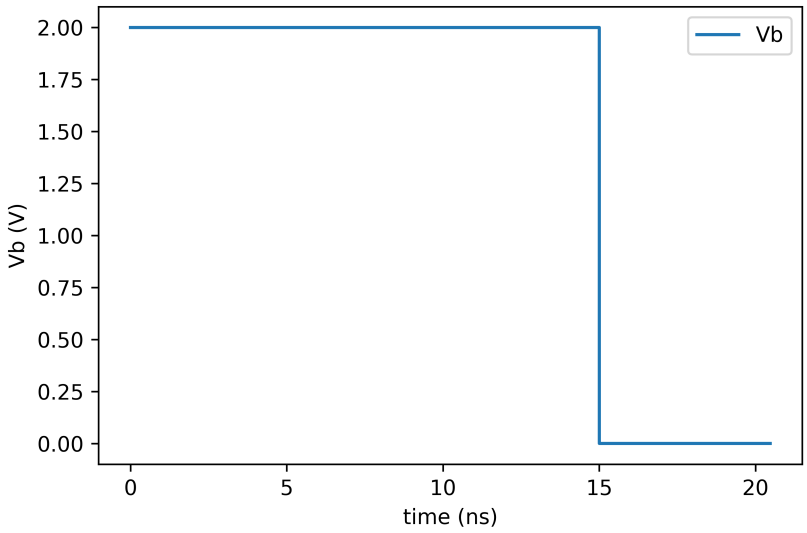

Figure 4.2: The voltage pulse used to reduce the energy barrier for voltage only control.

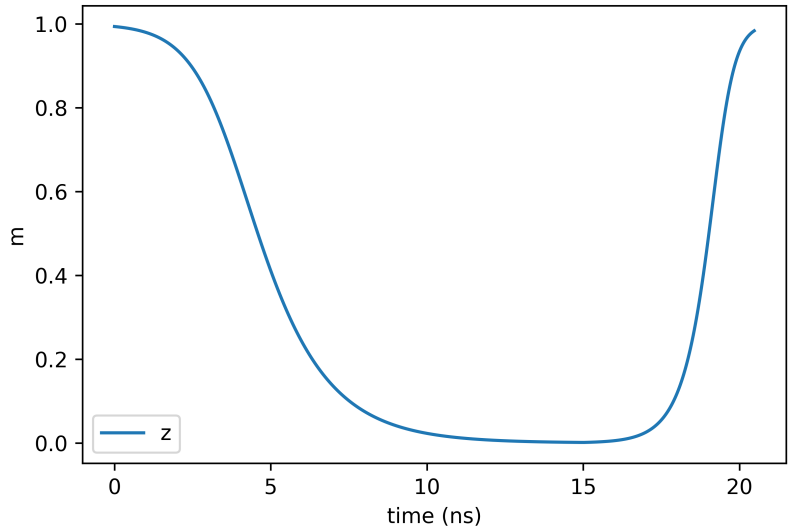

Figure 4.3: The z component of the normalized magnetization vector **m** for $1 \rightarrow$ -1 switching.

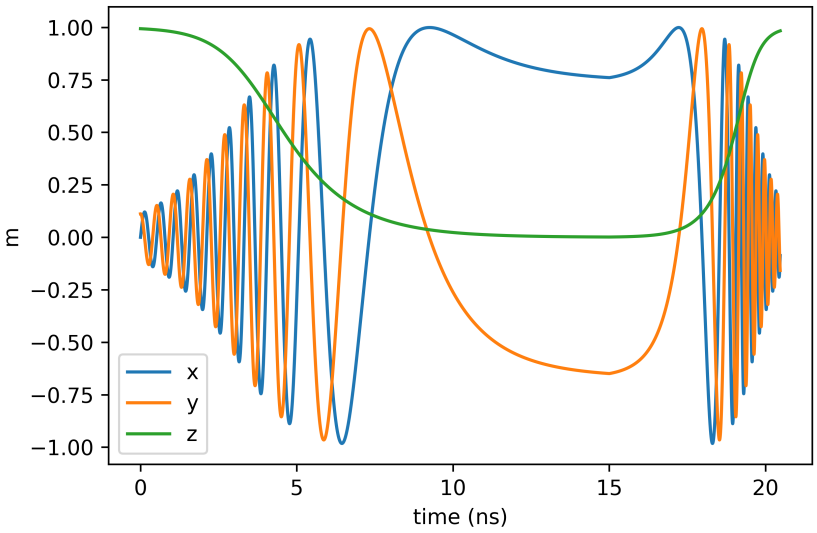

Figure 4.4: The normalized magnetization vector **m** and its Cartesian components for 1 → -1 switching.

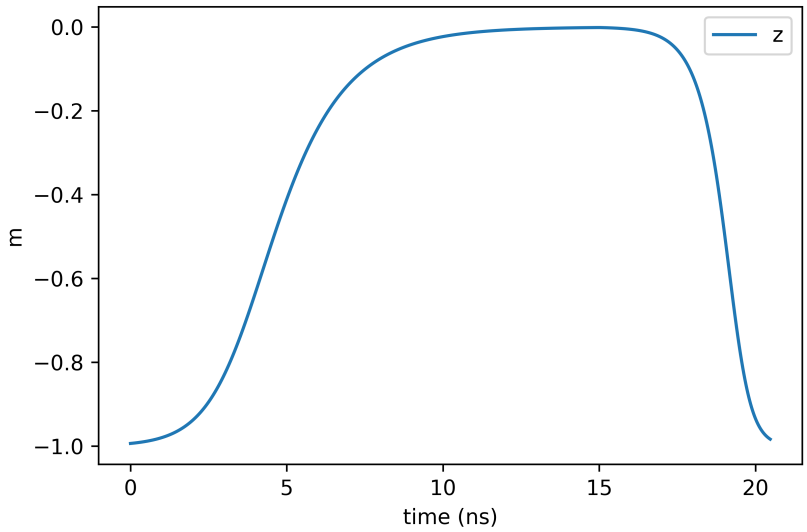

Figure 4.5: The z component of the normalized magnetization vector **m** for -1 → 1 switching.

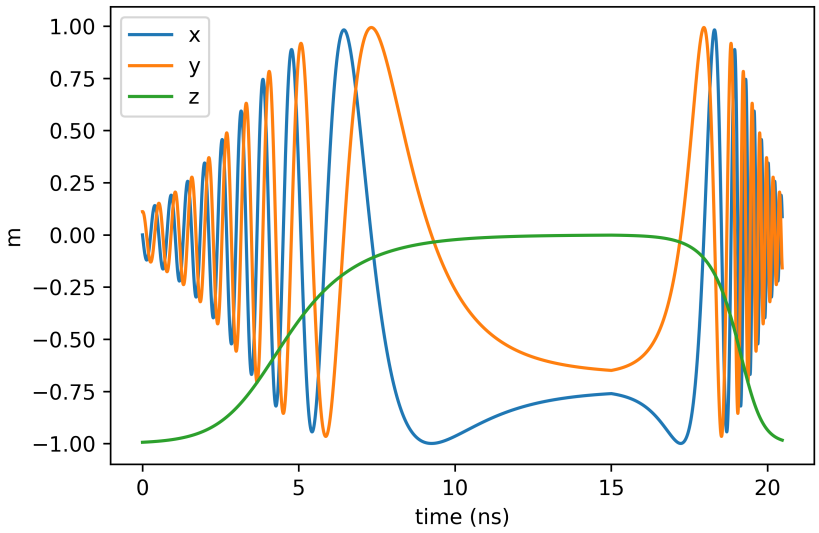

Figure 4.6: The normalized magnetization vector **m** and its Cartesian components for -1 $\rightarrow$ 1 switching.

4.3.2 Precessional Switching with an External In-Plane Magnetic Field

I apply an external in-plane magnetic field with magnitude $H_{app} = 9.6 \times 10^4$A/m with a precisely timed voltage pulse at 1.8V $> V_c$ to simulate precessional behavior like in Kang [22]. I am able to switch, but it is very hard to time the pulse precise enough to have reliable results.

Figures 4.7 – 4.8 contain the behavior for an oscillatory PMA to IMA transition without a shut off to switch. Figures 4.9 – 4.11 contain the behavior for a $z = 1$ to $z =$ -1 switch, while Figures 4.12 – 4.14 contain the behavior for a $z =$ -1 to $z = 1$ switch.

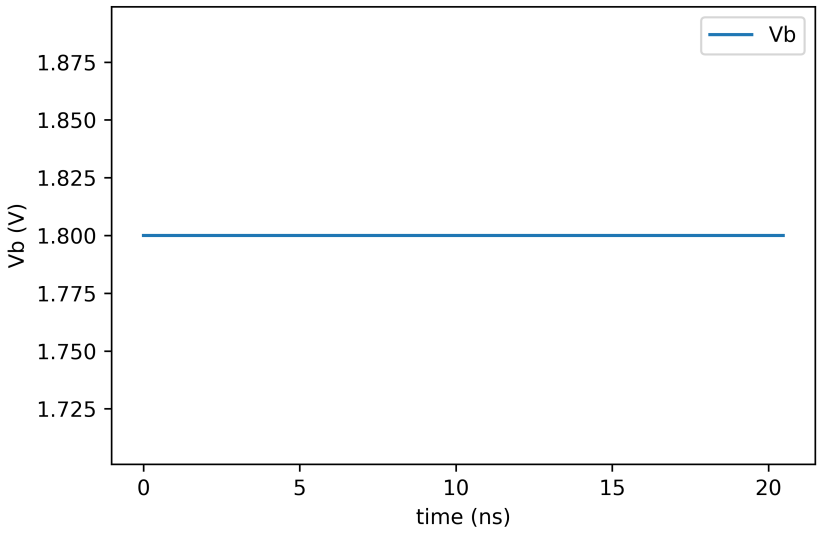

Figure 4.7: The voltage pulse used to reduce the energy barrier for precessional switching for continuous oscillatory behavior.

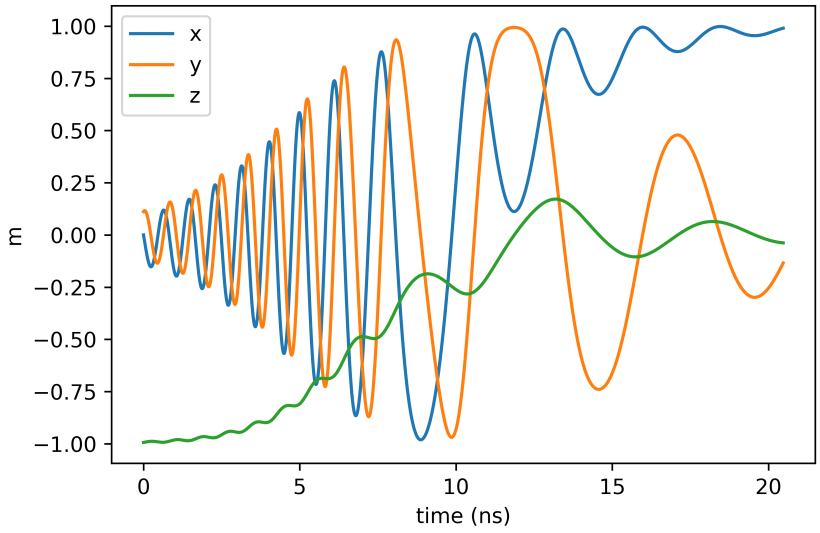

Figure 4.8: Transition from PMA to IMA for a magnet under an external magnetic field.

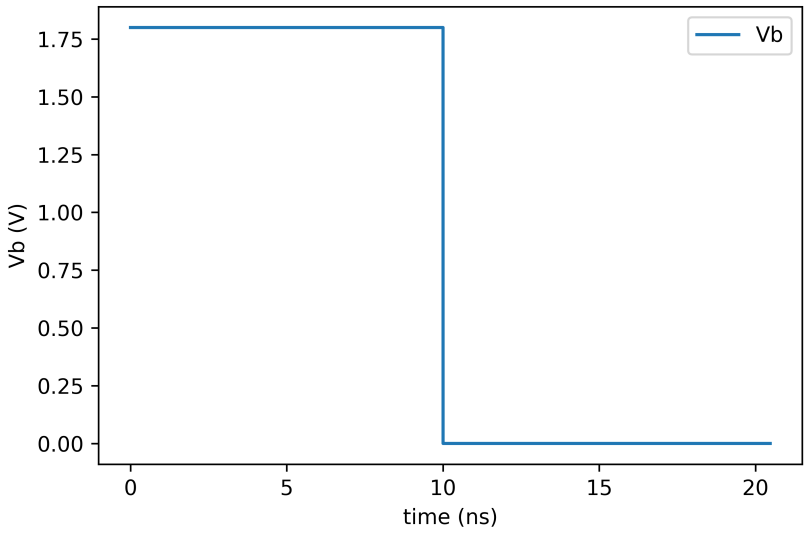

Figure 4.9: The voltage pulse used to reduce the energy barrier for precessional switching for 1 to -1 switching.

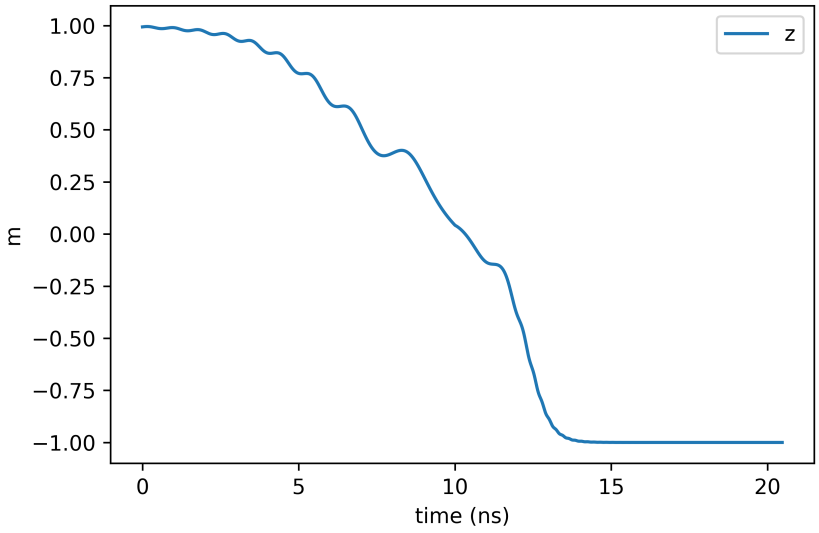

Figure 4.10: The z component of the normalized magnetization vector $\mathbf{m}$ for 1 $\rightarrow$ -1 switching under external field.

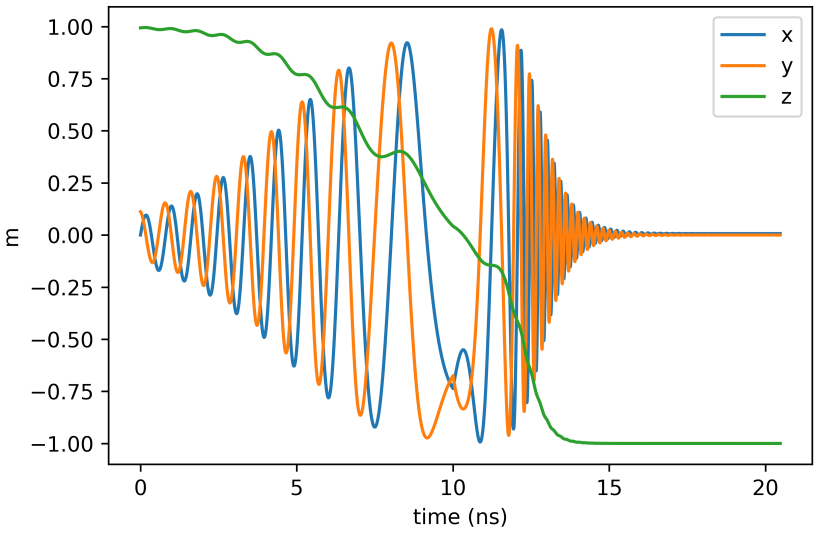

Figure 4.11: The normalized magnetization vector **m** and its Cartesian components for 1 → -1 switching under external field.

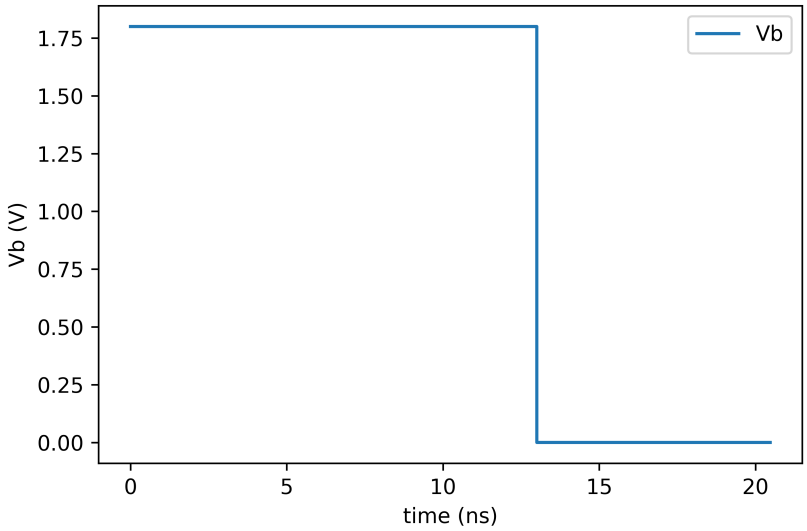

Figure 4.12: The voltage pulse used to reduce the energy barrier for precessional switching for -1 to 1 switching.

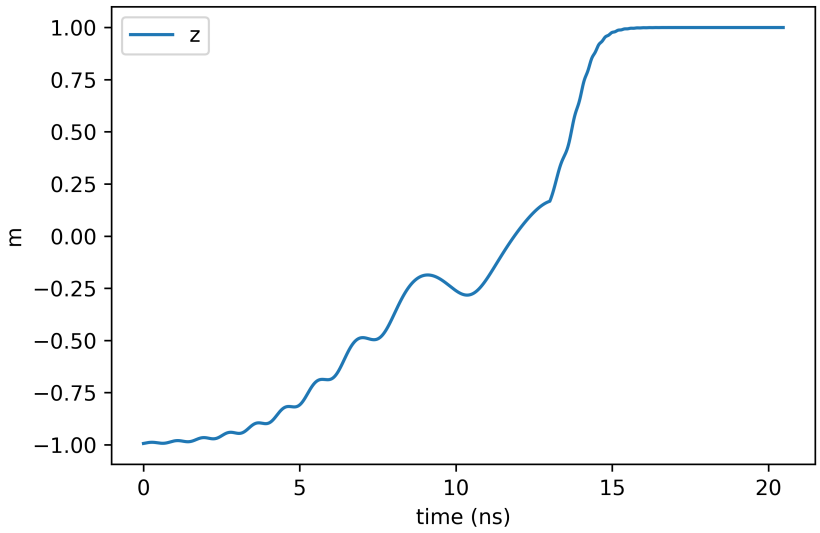

Figure 4.13: The z component of the normalized magnetization vector **m** for -1 $\rightarrow$ 1 switching under external field.

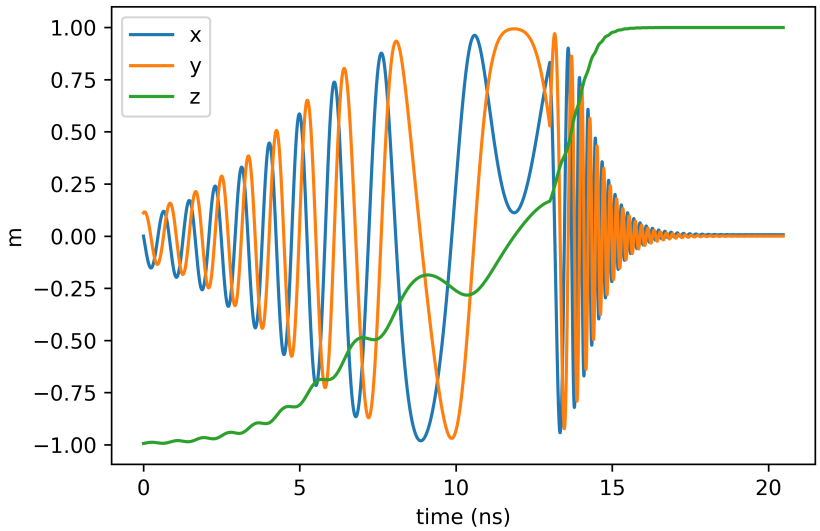

Figure 4.14: The normalized magnetization vector **m** and its Cartesian components for -1 $\rightarrow$ 1 switching under external field.

4.3.3 Thermally Assisted Switching

For thermally assisted switching of the magnet, I operated under the $V_b < V_c$ regime while simultaneously passing a current to torque the device. Due to VCMA reducing the energy barrier, I was able to switch magnetizations both

ways with a $I < I_c0(0\text{V})$ current that is less than the non-VCMA critical current. Equation 3.20 can be used to calculate the new effective critical current to determine optimal values to save energy consumption.

Figure 4.15 contains the plot for the VCMA voltage pulse that is used to switch in either direction. Figures 4.16 – 4.18 contain the plots for switching from the $z = 1$ to the $z = -1$ direction, while Figures 4.19 – 4.21 contain the plots for switching from the $z = -1$ to the $z = 1$ direction.

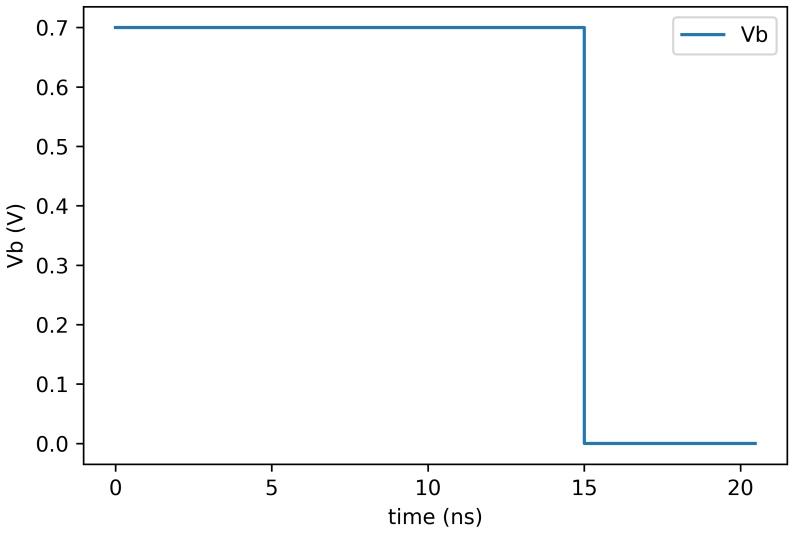

Figure 4.15: The voltage pulse used to reduce the energy barrier for thermally assisted switching.

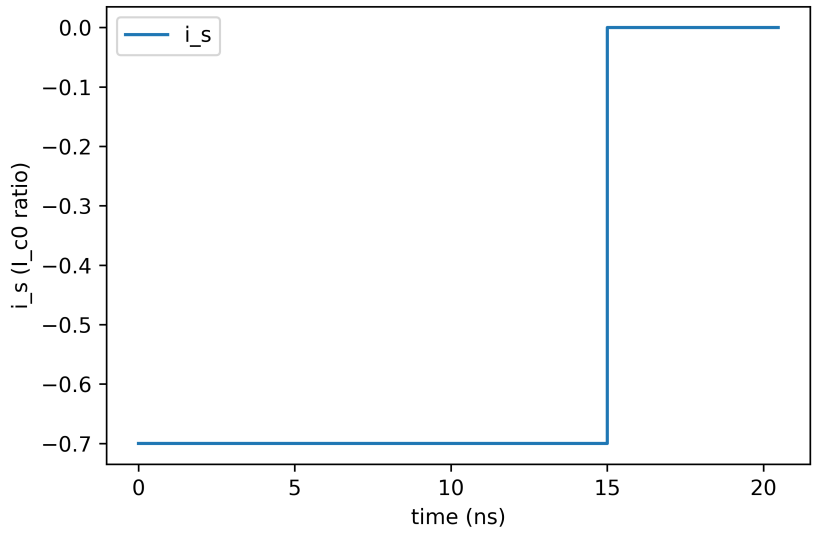

Figure 4.16: The current pulse used to switch for 1 to -1 switching under thermally assisted switching in a ratio of non-VCMA critical current.

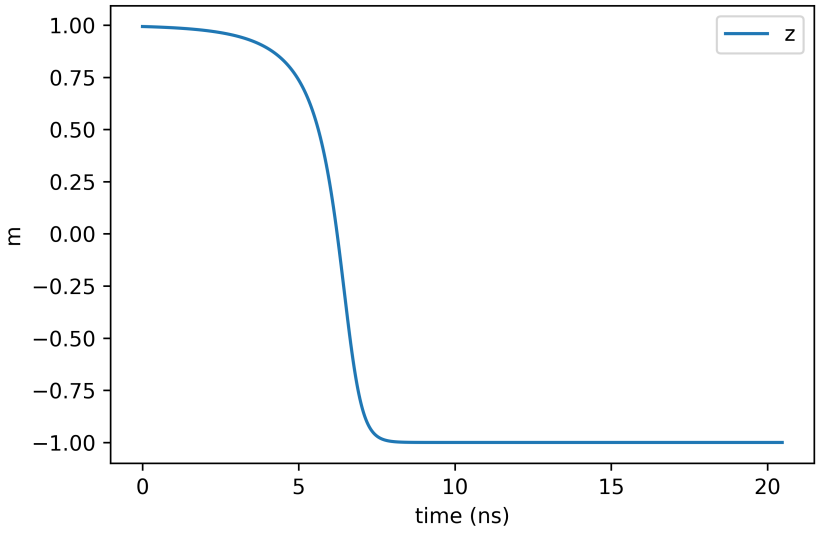

Figure 4.17: The z component of the normalized magnetization vector $\mathbf{m}$ for 1 $\rightarrow$ -1 switching under thermally assisted switching.

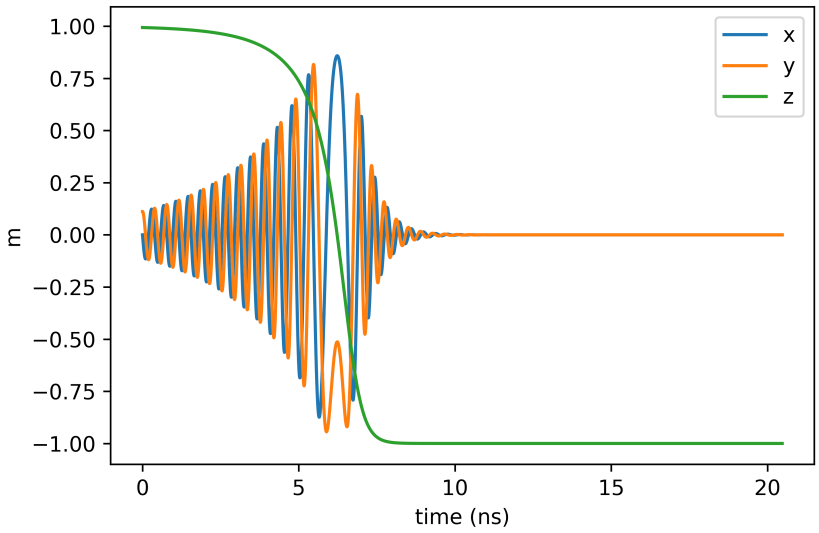

Figure 4.18: The normalized magnetization vector **m** and its Cartesian components for 1 → -1 switching under thermally assisted switching.

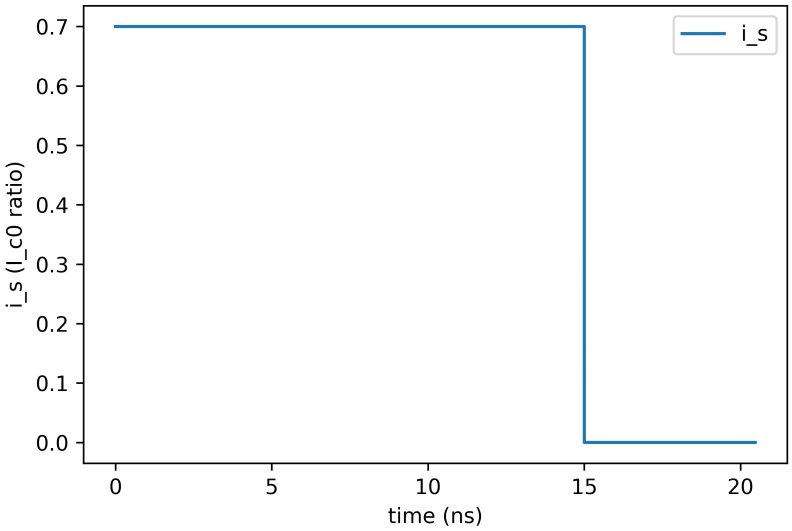

Figure 4.19: The current pulse used to switch for -1 to 1 switching under thermally assisted switching in a ratio of non-VCMA critical current.

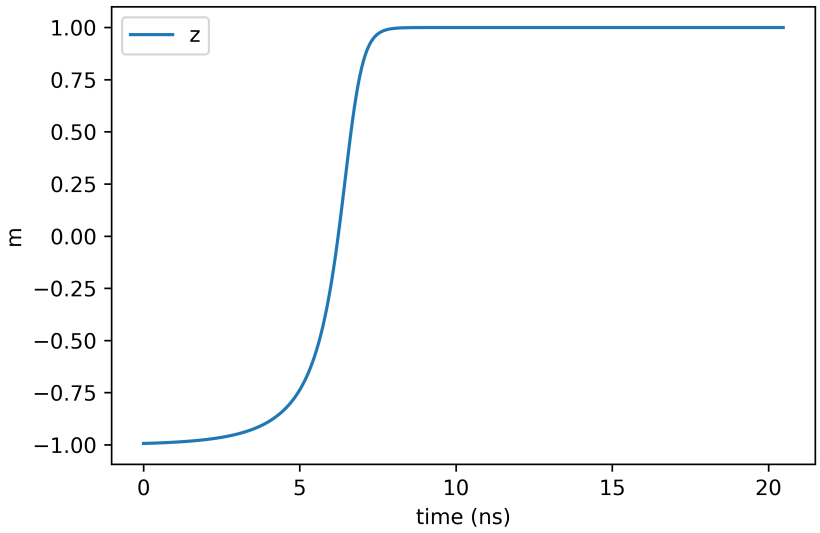

Figure 4.20: The z component of the normalized magnetization vector **m** for -1 $\rightarrow$ 1 switching under thermally assisted switching.

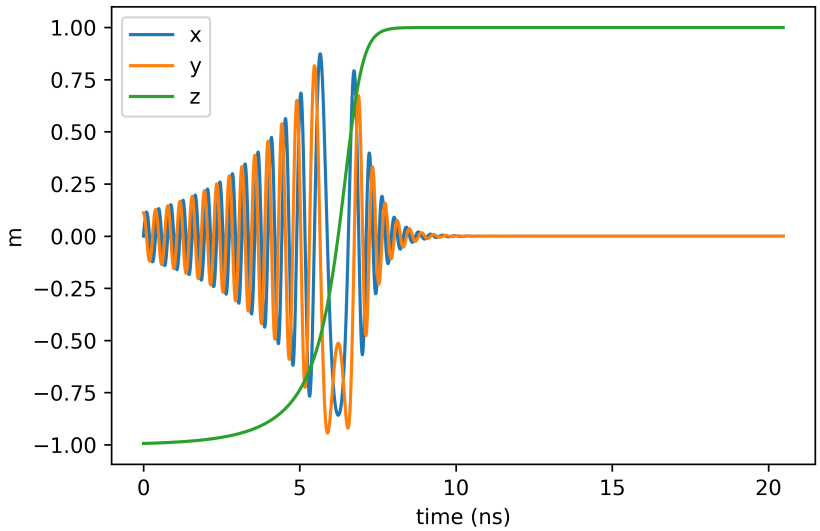

Figure 4.21: The normalized magnetization vector **m** and its Cartesian components for -1 $\rightarrow$ 1 switching under thermally assisted switching.

4.3.4 Voltage Controlled Magnetic Anisotropy with Current Assisted Switching

In these simulations, I first apply a VCMA voltage pulse, and then apply a separate current pulse after the first voltage pulse is finished. In order for

this to switch states, $V_b > V_c$, and the magnetization must move from its original state toward an in-plane orientation. An angular dependent critical current from Equation 3.23 must then switch the magnet after the E_b has been raised again and the magnetization is in the process of settling.

For STT assisted VCMA switching, figure 4.22 contains the plot for the VCMA voltage pulse that is used to switch in either direction. Figures 4.23 – 4.25 contain the plots for switching from the $z = 1$ to the $z = -1$ direction, while Figures 4.26 – 4.28 contain the plots for switching from the $z = -1$ to the $z = 1$ direction.

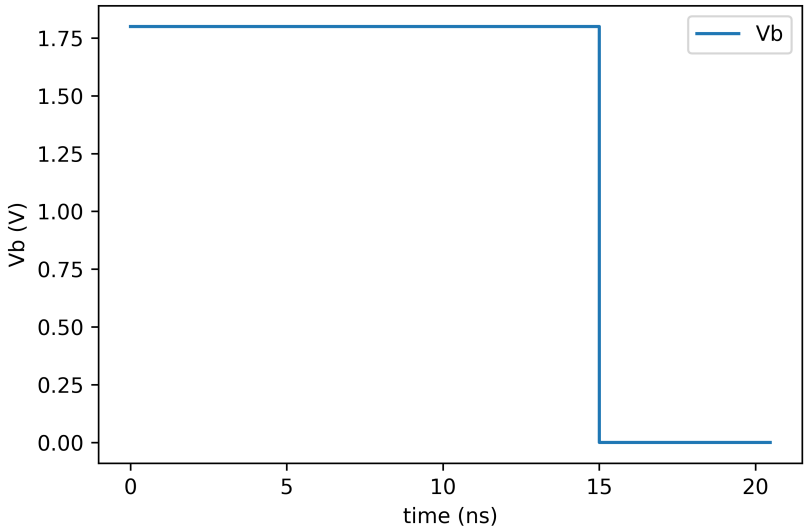

Figure 4.22: The voltage pulse used to reduce the energy barrier for spin current assisted switching.

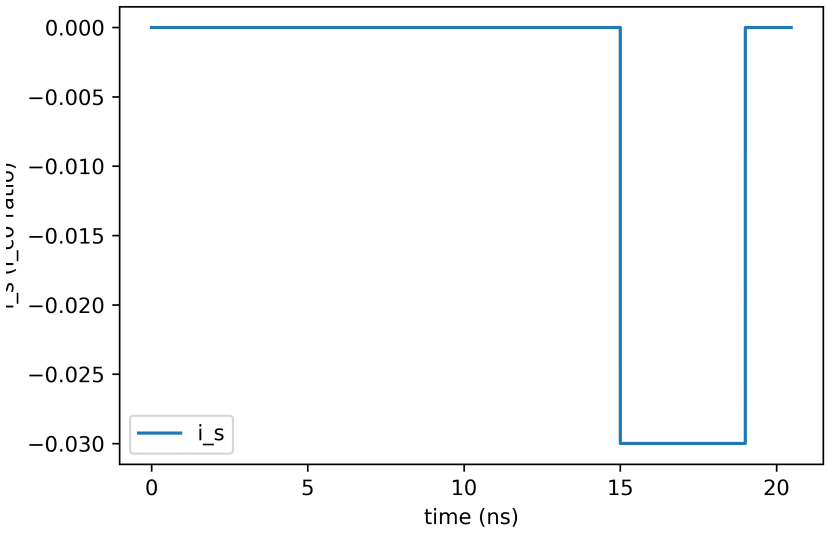

Figure 4.23: The current pulse used to switch for 1 to -1 switching under current assisted switching in a ratio of non-VCMA critical current.

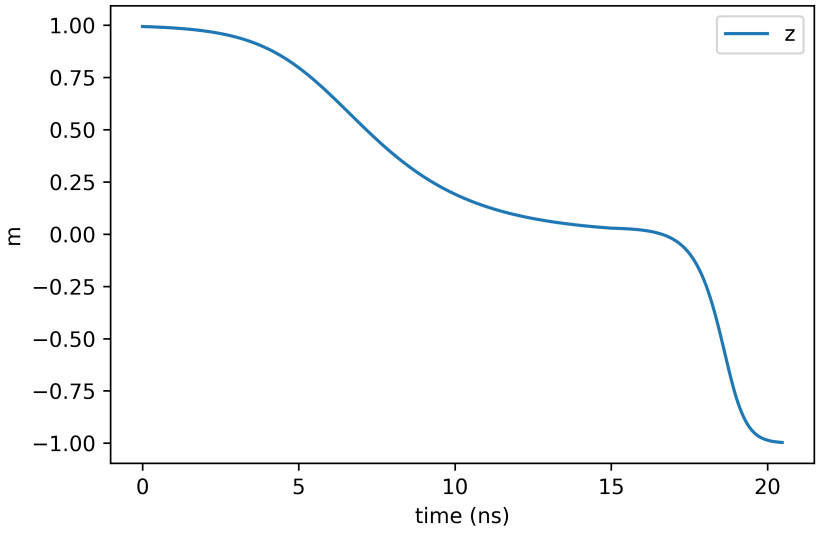

Figure 4.24: The z component of the normalized magnetization vector $\mathbf{m}$ for 1 $\rightarrow$ -1 switching under current assisted switching.

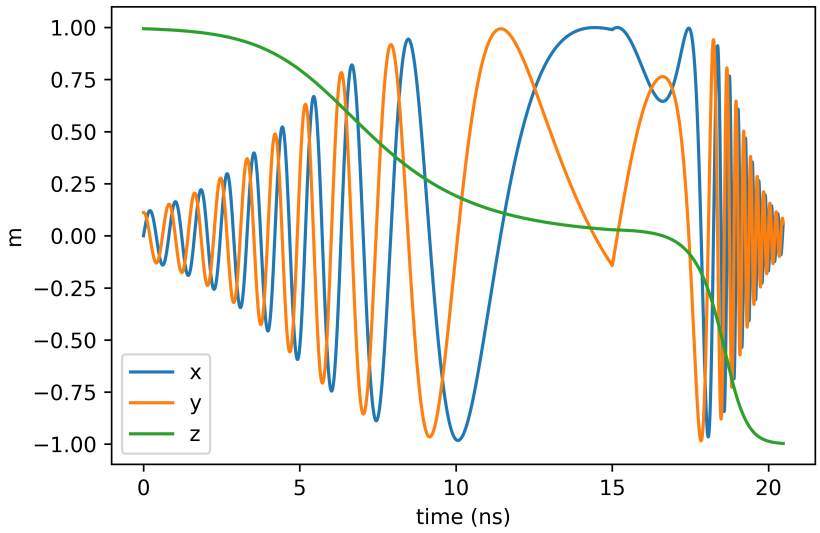

Figure 4.25: The normalized magnetization vector **m** and its Cartesian components for 1 → -1 switching under current assisted switching.

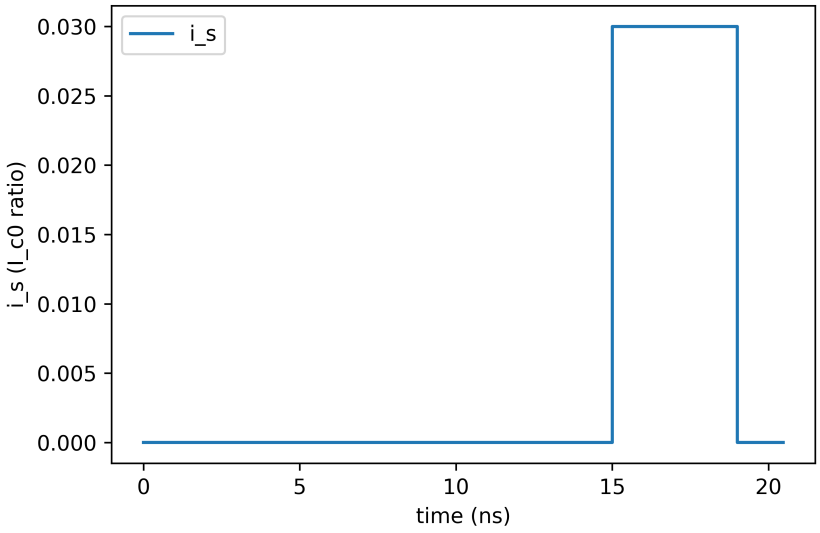

Figure 4.26: The current pulse used to switch for -1 to 1 switching under current assisted switching in a ratio of non-VCMA critical current.

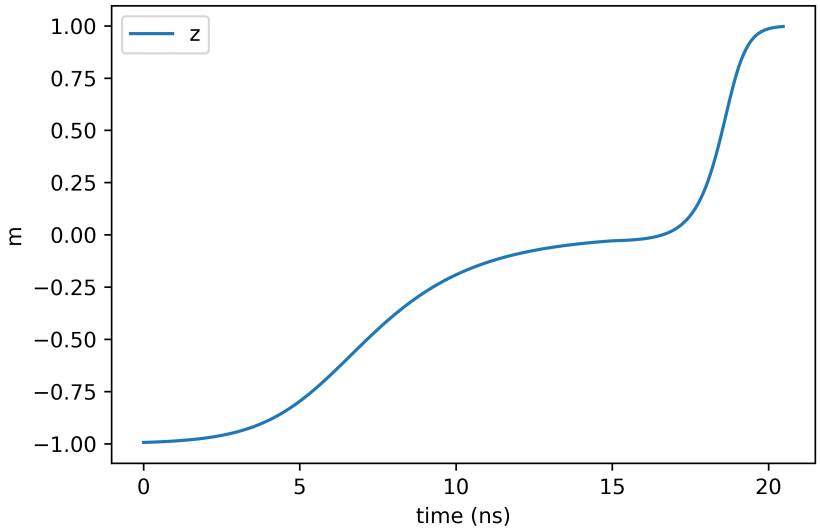

Figure 4.27: The z component of the normalized magnetization vector **m** for -1 → 1 switching under current assisted switching.

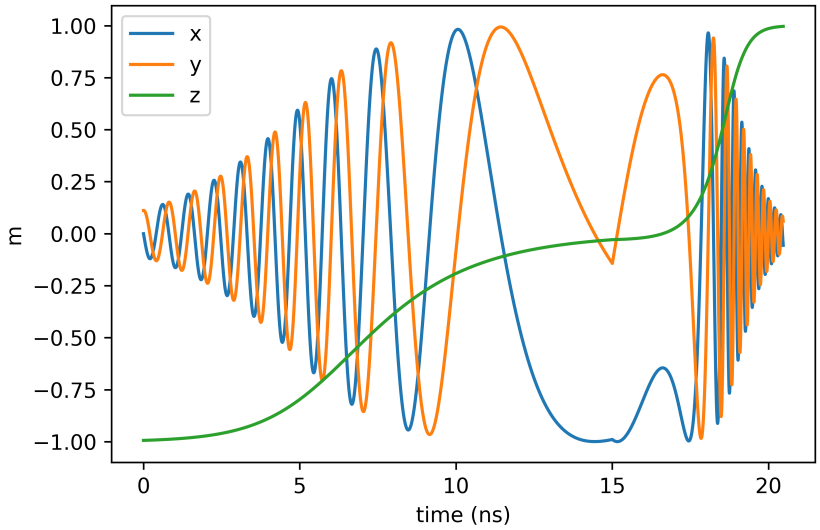

Figure 4.28: The normalized magnetization vector **m** and its Cartesian components for -1 → 1 switching under current assisted switching.

CHAPTER 5

CONCLUSIONS AND FUTURE WORK

In this work, I explored the qualitative behavioral results of VCMA and STT, and I was able to demonstrate three types of VCMA switching behavior. There is still a lot, however, that needs to be addressed. For starts, my torque currents and VCMA voltages were not coupled together. This coupling is non-negligible and should be done with modelling a resistance across the MTJ stack to determine a STT current [36], [37], [38].

What is perhaps more troublesome is the fact that my simulation results do not fully match the results from Kang with identical parameter values [22]. Our values for the thermal stability factor do not align, and his simulations have more waves and stronger precessional behaviors. Furthermore, the speed at which his devices switch is much greater than the speed of my simulations, which is extremely surprising. I propose some solutions to determine the source of error, or to make my simulations more accurate. The first is the slow damping of the magnetization direction toward the H_{eff} field direction, which eventually stops procession in my simulations altogether due to how close the componenets get. Without any initial angle, it is impossible to switch the magnet, which is what happens in the middle of my simulation if the magnetization direction and the effective field become too close. This issue can potentially be addressed through thermal effects or pseudothermal effects (for example, adding a constant non-zero thermal disturbance) [39]. Another potential fix to this solution would be to attempt and simulate the magnetization effects in spherical coordinates instead of Cartesian coordinates.

For one specific regime – the case where $V_b > V_c$ and a spin current torque exists in the device – I believe my simulations to be inaccurate according to data from other sources. VCMA precessional effects supposedly should

dominate STT/SOT effects for high voltages [35], [40], [41], [42], yet I saw in my simulations that the magnets easily switched under small currents while $V_b > V_c$ as I had an almost non-existant precessional contribution toward the LLGS equation in my simulations. In theory, my MRAM device should somehow not switch under large VCMA effects for $V_b > V_c$. I pose a few questions that can potentially help resolve these inaccuracies. Does the anisotropy under the orbital hall effect convert to a larger in-plane magnetic field due to shifting preference of perpendicular orbits to in-plane orbits? In other words, does the orbital hall effect not only reduce the perpendicular anisotropy, but also increase the in-plane anisotropy? It is also unclear to me what happens for $V_b > V_c$. Does this anisotropy decrease stop at the interfacial anisotropy coefficient $K_i = 0$, or does it continue to decrease into the negatives and cause significant change in a negative H_{eff}?

Some other factors that should be considered are the field-like torque, and ensuring that the voltage remains within dielectric breakdown levels. Popular orientations for VCMA nowadays with proven experimental results include external magnetic fields in the perpendicular direction that can switch under unidirections STT voltages, and should be considered more in future research [43].

Potential areas of future research can include multiferroic devices; devices that exhibit both VCMA and ferroelectric effects with the same materials. Completing the compact modeling and comparing results to other technologies can also be insightful, especially if comparing the IBM's recent VTFET silicon technology. Finally, antiferromagnets and ferrimagnets can potentially open up larger realms of possibilites and even cause faster switching.

REFERENCES

[1] Q. Shao, P. Li, L. Liu, H. Yang, S. Fukami, A. Razavi, H. Wu, F. Freimuth, Y. Mokrousov, M. D. Stiles et al., "Roadmap of spin-orbit torques," *IEEE Transactions on Magnetics*, 2021.

[2] N. S. Kim, T. Austin, D. Baauw, T. Mudge, K. Flautner, J. S. Hu, M. J. Irwin, M. Kandemir, and V. Narayanan, "Leakage current: Moore's law meets static power," *computer*, vol. 36, no. 12, pp. 68–75, 2003.

[3] M. Lundstrom, "Moore's law forever?" *Science*, vol. 299, no. 5604, pp. 210–211, 2003.

[4] H.-S. P. Wong and S. Salahuddin, "Memory leads the way to better computing," *Nature nanotechnology*, vol. 10, no. 3, pp. 191–194, 2015.

[5] A. D. Kent and D. C. Worledge, "A new spin on magnetic memories," *Nature nanotechnology*, vol. 10, no. 3, pp. 187–191, 2015.

[6] H. Liu, "Spin transfer driven magnetization dynamics in spin valves and magnetic tunnel junctions," Ph.D. dissertation, New York University, 2013.

[7] G. Binasch, P. Grünberg, F. Saurenbach, and W. Zinn, "Enhanced magnetoresistance in layered magnetic structures with antiferromagnetic interlayer exchange," *Physical review B*, vol. 39, no. 7, p. 4828, 1989.

[8] M. N. Baibich, J. M. Broto, A. Fert, F. N. Van Dau, F. Petroff, P. Etienne, G. Creuzet, A. Friederich, and J. Chazelas, "Giant magnetoresistance of (001) fe/(001) cr magnetic superlattices," *Physical review letters*, vol. 61, no. 21, p. 2472, 1988.

[9] M. Julliere, "Tunneling between ferromagnetic films," *Physics letters A*, vol. 54, no. 3, pp. 225–226, 1975.

[10] R. Mertens, "MS Windows NT kernel description," https://www.mram-info.com/introduction, accessed: 2022-05-01.

[11] J. Z. Sun, "Spin angular momentum transfer in current-perpendicular nanomagnetic junctions," *IBM journal of research and development*, vol. 50, no. 1, pp. 81–100, 2006.

[12] A. Manchon, J. Železnỳ, I. M. Miron, T. Jungwirth, J. Sinova, A. Thiaville, K. Garello, and P. Gambardella, "Current-induced spin-orbit torques in ferromagnetic and antiferromagnetic systems," *Reviews of Modern Physics*, vol. 91, no. 3, p. 035004, 2019.

[13] J. Alzate, "Voltage-controlled magnetic dynamics in nanoscale magnetic tunnel junctions," *Electrical Engineering, University of California, Los Angeles*, 2014.

[14] B. Rana and Y. Otani, "Towards magnonic devices based on voltage-controlled magnetic anisotropy," *Communications Physics*, vol. 2, no. 1, pp. 1–12, 2019.

[15] J. M. Coey, *Magnetism and magnetic materials*. Cambridge university press, 2010.

[16] K. M. Krishnan, *Fundamentals and applications of magnetic materials*. Oxford University Press, 2016.

[17] B. D. Cullity and C. D. Graham, *Introduction to magnetic materials*. John Wiley & Sons, 2011.

[18] M. Sato and Y. Ishii, "Simple and approximate expressions of demagnetizing factors of uniformly magnetized rectangular rod and cylinder," *Journal of Applied Physics*, vol. 66, no. 2, pp. 983–985, 1989.

[19] M. Beleggia, M. De Graef, Y. T. Millev, D. A. Goode, and G. Rowlands, "Demagnetization factors for elliptic cylinders," *Journal of Physics D: Applied Physics*, vol. 38, no. 18, p. 3333, 2005.

[20] D.-X. Chen, E. Pardo, and A. Sanchez, "Fluxmetric and magnetometric demagnetizing factors for cylinders," *Journal of Magnetism and Magnetic Materials*, vol. 306, no. 1, pp. 135–146, 2006.

[21] J. Osborn, "Demagnetizing factors of the general ellipsoid," *Physical review*, vol. 67, no. 11-12, p. 351, 1945.

[22] W. Kang, Y. Ran, Y. Zhang, W. Lv, and W. Zhao, "Modeling and exploration of the voltage-controlled magnetic anisotropy effect for the next-generation low-power and high-speed mram applications," *IEEE Transactions on Nanotechnology*, vol. 16, no. 3, pp. 387–395, 2017.

[23] V. Naik, H. Meng, J. Xiao, R. Liu, A. Kumar, K. Zeng, P. Luo, and S. Yap, "Effect of electric-field on the perpendicular magnetic anisotropy and strain properties in cofeb/mgo magnetic tunnel junctions," *Applied Physics Letters*, vol. 105, no. 5, p. 052403, 2014.

[24] S. E. Barnes, J. Ieda, and S. Maekawa, "Rashba spin-orbit anisotropy and the electric field control of magnetism," *Scientific reports*, vol. 4, no. 1, pp. 1–5, 2014.

[25] C.-G. Duan, S. S. Jaswal, and E. Y. Tsymbal, "Predicted magnetoelectric effect in fe/batio 3 multilayers: ferroelectric control of magnetism," *Physical Review Letters*, vol. 97, no. 4, p. 047201, 2006.

[26] S. H. Simon, *The Oxford solid state basics*. OUP Oxford, 2013.

[27] J. Sun, "Resistance-area product and size dependence of spin-torque switching efficiency in cofeb-mgo based magnetic tunnel junctions," *Physical Review B*, vol. 96, no. 6, p. 064437, 2017.

[28] S. Yuasa and D. Djayaprawira, "Giant tunnel magnetoresistance in magnetic tunnel junctions with a crystalline mgo (0 0 1) barrier," *Journal of Physics D: Applied Physics*, vol. 40, no. 21, p. R337, 2007.

[29] Y. Zhang, W. Zhao, Y. Lakys, J.-O. Klein, J.-V. Kim, D. Ravelosona, and C. Chappert, "Compact modeling of perpendicular-anisotropy cofeb/mgo magnetic tunnel junctions," *IEEE transactions on Electron devices*, vol. 59, no. 3, pp. 819–826, 2012.

[30] S. Ament, N. Rangarajan, and S. Rakheja, "A practical guide to solving the stochastic landau-lifshitz-gilbert-slonczewski equation for macrospin dynamics," *Journal of Computational Physics (submitted)*, 2016.

[31] S. Miwa, M. Suzuki, M. Tsujikawa, K. Matsuda, T. Nozaki, K. Tanaka, T. Tsukahara, K. Nawaoka, M. Goto, Y. Kotani et al., "Voltage controlled interfacial magnetism through platinum orbits," *Nature communications*, vol. 8, no. 1, pp. 1–9, 2017.

[32] C.-G. Duan, J. P. Velev, R. F. Sabirianov, Z. Zhu, J. Chu, S. S. Jaswal, and E. Y. Tsymbal, "Surface magnetoelectric effect in ferromagnetic metal films," *Physical review letters*, vol. 101, no. 13, p. 137201, 2008.

[33] D. Dimitrov, Z. Gao, X. Wang, W. Jung, X. Lou, and O. G. Heinonen, "Dielectric breakdown of mgo magnetic tunnel junctions," *Applied Physics Letters*, vol. 94, no. 12, p. 123110, 2009.

[34] C. Yoshida, M. Kurasawa, Y. M. Lee, K. Tsunoda, M. Aoki, and Y. Sugiyama, "A study of dielectric breakdown mechanism in cofeb/mgo/cofeb magnetic tunnel junction," in *2009 IEEE International Reliability Physics Symposium*. IEEE, 2009, pp. 139–142.

[35] S. Kanai, Y. Nakatani, M. Yamanouchi, S. Ikeda, H. Sato, F. Matsukura, and H. Ohno, "Magnetization switching in a cofeb/mgo magnetic tunnel junction by combining spin-transfer torque and electric field-effect," *Applied Physics Letters*, vol. 104, no. 21, p. 212406, 2014.

[36] W. Brinkman, R. Dynes, and J. Rowell, "Tunneling conductance of asymmetrical barriers," *Journal of applied physics*, vol. 41, no. 5, pp. 1915–1921, 1970.

[37] Y. Zhang, B. Yan, W. Kang, Y. Cheng, J.-O. Klein, Y. Zhang, Y. Chen, and W. Zhao, "Compact model of subvolume mtj and its design application at nanoscale technology nodes," *IEEE Transactions on Electron Devices*, vol. 62, no. 6, pp. 2048–2055, 2015.

[38] J. C. Slonczewski, "Conductance and exchange coupling of two ferromagnets separated by a tunneling barrier," *Physical Review B*, vol. 39, no. 10, p. 6995, 1989.

[39] F. Garcia-Redondo, P. Prabhat, M. Bhargava, and C. Dray, "A compact model for scalable mtj simulation," in *SMACD/PRIME 2021; International Conference on SMACD and 16th Conference on PRIME*. VDE, 2021, pp. 1–4.

[40] M. Endo, S. Kanai, S. Ikeda, F. Matsukura, and H. Ohno, "Electric-field effects on thickness dependent magnetic anisotropy of sputtered mgo/co 40 fe 40 b 20/ta structures," *Applied Physics Letters*, vol. 96, no. 21, p. 212503, 2010.

[41] S. Kanai, M. Yamanouchi, S. Ikeda, Y. Nakatani, F. Matsukura, and H. Ohno, "Electric field-induced magnetization reversal in a perpendicular-anisotropy cofeb-mgo magnetic tunnel junction," *Applied Physics Letters*, vol. 101, no. 12, p. 122403, 2012.

[42] S. Kanai, Y. Nakatani, M. Yamanouchi, S. Ikeda, F. Matsukura, and H. Ohno, "In-plane magnetic field dependence of electric field-induced magnetization switching," *Applied Physics Letters*, vol. 103, no. 7, p. 072408, 2013.

[43] Y. C. Wu, "High speed mram with voltage control of magnetic anisotropy (vcma) effect," 2021.